Composites Part A 112 (2018) 525–538

Contents lists available at ScienceDirect

Composites Part A

journal homepage: www.elsevier.com/locate/compositesa

Continuous carbon nanotube synthesis on charged carbon fibers

David B. Anthony[a,b,c], XiaoMeng Sui[d], Israel Kellersztein[d], Hugo G. De Luca[a], Edward R. White[a], H. Daniel Wagner[d], Emile S. Greenhalgh[c], Alexander Bismarck[b,e], Milo S.P. Shaffer[a,*]

[a] Nanostructured Hierarchical Assemblies and Composites (NanoHAC) Group, Department of Chemistry, Imperial College London, South Kensington Campus, London SW7 2AZ, UK
[b] Polymer and Composite Engineering (PaCE) Group, Department of Chemical Engineering, Imperial College London, South Kensington Campus, London SW7 2AZ, UK
[c] The Composites Centre, Department of Aeronautics, Imperial College London, South Kensington Campus, London SW7 2AZ, UK
[d] Department of Materials and Interfaces, Weizmann Institute of Science, Rehovot 76100, Israel
[e] Polymer and Composite Engineering (PaCE) Group, Institute of Materials Chemistry and Research, Facility of Chemistry, University of Vienna, Währinger Str. 42, A-1090 Vienna, Austria

ARTICLE INFO

Keywords:
A. Carbon nanotubes and nanofibers
A. Carbon fibers
B. Fiber/matrix bond
E. Chemical vapor deposition

ABSTRACT

Carbon nanotube grafted carbon fibers (CNT-g-CFs) were prepared continuously, spool to spool, via thermal CVD. The application of an in-situ potential difference (300 V), between the fibers and a cylindrical graphite foil counter electrode, enhanced the growth, producing a uniform coverage of carbon nanotubes with diameter ca. 10 nm and length ca. 125 nm. Single fiber tensile tests show that this approach avoids the significant reduction of the underlying carbon fiber strengths, which is usually associated with CVD grafting processes. Single fiber fragmentation tests in epoxy, with *in-situ* video fragment detection, demonstrated that the CNT-g-CFs have the highest interfacial shear strength reported for such systems (101 ± 5 MPa), comparable to state-of-the-art sizing controls (103 ± 8 MPa). Single fiber pull-out data show similar trends. The short length of the grafted CNTs is particularly attractive for retaining the volume fraction of the primary fibers in composite applications. The results are compared with a short review of the interfacial data available for related systems.

1. Introduction

Carbon fiber reinforced composites (CFRCs) are widely used for their high specific strength and modulus [1] in an extensive range of industries. CFRCs possess excellent in-plane tensile properties but designs are often limited by interlaminar and compressive performance [2]. The introduction of carbon nanotubes (CNTs) into composites can enhance through thickness matrix dominated properties, in the intralaminar and interlaminar regions, without affecting in-plane performance [3]. CNTs can also enhance through thickness electrical and thermal conductivities in CFRCs. The addition of CNTs dispersed in the matrix can be effective at low concentrations, but is limited by increased matrix viscosity and/or filtration effects [4]. As an alternative, CNTs can be directly grafted onto carbon fibers (CNT-g-CFs), during synthesis, to form a hierarchical reinforcement, combining nanoscale and microscale reinforcements. Computational models of this type of hierarchical composite predict a net benefit when CNTs are present at the fiber surface [5–10], through diffusion of stresses across the critical fiber-matrix region, as found in some biological systems [10]. Another motivation for including CNTs in composites is to create a conductive network which can be used for *in-situ* damage detection [11,12]. Mechanical properties of CFRCs, and hierarchical composites, are primarily determined by fiber volume fractions; grafting long CNTs onto the fiber surfaces increase fiber-fiber separation [13] resulting in a reduced fiber packing. An "ideal" perpendicular CNT grafting length can therefore be suggested, which does not affect the fiber volume fraction (Fig. 1 and supplementary information (SI) S1). To maintain a fiber volume fraction of 60% for a typical aerospace grade* carbon fibers with diameters (d) of 7 μm requires the fiber-fiber separation to be 1.6 μm or lower (approx. $d/4.4$).

Current methods for producing CNT-grafted fibers (also known as hairy [3,14,15] or fuzzy fibers [6,13,16]) tend to produce excessively long grafted CNTs. In addition, the chemical vapor deposition (CVD) synthesis is typically limited to small scale batch processing due to the

* Corresponding author.
E-mail addresses: d.anthony08@imperial.ac.uk (D.B. Anthony), xiaomeng.sui@weizmann.ac.il (X. Sui), israel.kellersztein@weizmann.ac.il (I. Kellersztein), hugo.de-luca14@imperial.ac.uk (H.G. De Luca), daniel.wagner@weizmann.ac.il (H.D. Wagner), e.greenhalgh@imperial.ac.uk (E.S. Greenhalgh), a.bismarck@imperial.ac.uk (A. Bismarck), m.shaffer@imperial.ac.uk (M.S.P. Shaffer).
* Hexcel Composites. HexTow™ AS4 carbon fiber. Data Sheet. 2009:1–2.

https://doi.org/10.1016/j.compositesa.2018.05.027
Received 22 December 2017; Received in revised form 19 April 2018; Accepted 26 May 2018
Available online 28 May 2018
1359-835X/

Acronyms and symbols

$\overline{\sigma}_f$	average fiber stress
$\bar{l}$	average fragment length
$\bar{l}_{sat}$	average saturation fragmentation length
BET	Brunauer, Emmett and Teller
CFRC	carbon fiber reinforced composite
CNT-g-CF	carbon nanotube-grafted-carbon fiber
CNT	carbon nanotube
CVD	chemical vapor deposition
l_c	critical fiber length
l_e	embedded fiber length
A_e	embedded fiber area
FBPO	fiber bundle pull-out
d	fiber diameter
E_f	fiber modulus
d_f	fragmentation failure/pull-out fiber diameter
IFSS, τ_i, τ_{app}	interfacial shear strength
I_G/I_D	intensity ratio of the G-mode to the D-mode
L	length
E_m	matrix modulus
σ_m	measured stress
MD-SFPO	micro-droplet single fiber pull-out
F_{max}	peak pull-out force
PMMA	poly(methyl methacrylate)
PAN	polyacrylonitrile
PEEK	polyetheretherketone
P(VEAc)	polyvinylethylacetate
d_{tow}	pull-out tow diameter
l_{sat}	saturation fragmentation length
SEM	scanning electron microscope
SFFT	single fiber fragmentation test
SFPO	single fiber pull-out
SF-PushOut	single fiber push-out
Γ	standard Gamma function
SI	supplementary information
σ_f	tensile strength of fiber
TGA	thermal gravimetric analysis
TEM	transmission electron microscopy
$\overline{\sigma}_f(l_c)$	ultimate fiber strength at critical length
α	Weibull scale parameter
β	Weibull shape parameters/Weibull modulus

need for high temperatures (> 500 °C) and flammable gases (carbon feedstock, hydrogen). The largest batch CNT-g-CF samples are currently produced by grafting CNTs onto woven carbon fiber materials using traditional hot-walled CVD, with sample lengths limited to the size of the stable hot-zone [17]; tubular furnaces also require the woven fabric to be rolled or scrolled to maximize the volume of the material to be grafted. An unfortunate by-product of using a woven substrate is normally poor CNTs coverage between warp and weft yarn overlaid regions, which in some weave architectures can lead to a significant portion of the parent material left unmodified [18]. A further challenge is that the growth of CNTs on carbon fibers typically degrades the intrinsic strength and stiffness of the original structural fiber properties. The observed fiber damage is a result of the high CVD processing temperatures in the presence of a metallic catalyst required for the synthesis of CNTs. Potential degradation mechanisms include dissolution of carbon surface by the catalyst leading to channeling [19], and/or consumption of the carbon surface as a feedstock for CNT growth. Damage to the fiber can also be sustained from residual water/oxygen if present [20] or hydrogenation/gasification [21] particularly during catalyst reduction at elevated temperatures (> 500 °C); an increased channeling rate has been observed on graphite in a dry hydrogen rich atmosphere and to a lesser extent in wet hydrogen environments [19]. Retaining the mechanical properties of the pristine carbon fiber after batch CVD CNT-grafting has been reported by various means, including, reducing the temperature during CVD CNT-synthesis (ca. 500 °C) [22], as well as prolonged [23] or minimal [24,25] exposure to the CVD conditions. Optimized CNT-synthesis reaction gas stoichiometry [26] or tensioning fibers during CNT synthesis to reduce thermally-activated mechanochemical changes of the fiber microstructure [27] were also shown to limit damage of the carbon fiber substrate during CNT-synthesis. Alternatively, catalysts which do not readily dissociate carbon, for example ZrOCl [28] or Cu [29] can be used, although they tend to promote the growth carbon nanofibers with a herringbone or platelet structure rather than multi-walled carbon nanotubes. The most prevalent method to limit carbon fiber damage during the synthesis of CNT on carbon fiber substrates is the application of a barrier coating to the fiber surfaces, which limits catalyst contact with the fiber substrate. Common barrier coatings include silicon/silica [30–36], alumina [37–39] or pyrolytic carbon [40–42]. However, recently, we reported that the application of a modest potential difference minimized carbon fiber damage and improved the CNT coverage without the requirement for a barrier coating [43].

For practical evaluation and application in composites, CNT-grafted fibers should be produced on the tow level on a suitably large/continuous scale, ideally during fiber production. Continuous CNT-grafting at the fiber tow level has been reported for fibers that are more resilient to the harsh synthesis conditions, such alumina [44] and glass [35,45]. Nevertheless, carbon fibers are preferred in the majority of high performance structural applications, especially those that are specific stiffness driven. Two examples of manufacturing continuous CNT-g-CF have been reported; in both cases, the carbon fiber surfaces were protected by a pacifying siloxane based-coating. CFs grafted with ca. 2 μm CNTs [35] used in epoxy composites increased the interlaminar fracture toughness (G_{IC}, double cantilever beam) by 36%, relative to an unsized carbon fiber control; however, G_{IC} was affected by the length of the grafted CNTs due to the reduction in the fiber volume fraction with increasing CNT length. Craddock *et al.* [46] manufactured grafted CNTs with less than 5 μm in length onto spread tow carbon fibers using an injection CVD route. These CNT-g-CF were used to produce composites, which possessed a higher thermal diffusivity than the control composites made with desized carbon fibers. A recent article described the production of CNT-g-CF by injection-CVD, in multiple batch processes to achieve an extended CNT-g-CF tow product with CNTs length of ca. 1 μm [47]. The interlaminar shear strength (three-point bending) of epoxy matrix composites containing these CNT-g-CFs was 35% higher than that of the control specimens. Yet, in spite of these publications, the effect of continuous CNT-g-CF CVD synthesis on the fiber mechanical or fiber/matrix interfacial properties has not been well established.

The aim of the present study was to demonstrate a scalable manufacturing process to graft short CNTs onto carbon fibers in order to improve the interfacial properties, whilst avoiding any loss in fiber stiffness or strength. The application of a modest potential difference during CNT synthesis has been shown to be beneficial in batch CVD conditions, improving growth uniformity and minimizing damage to the fibers during processing. The strategy for increased production was to implement this methodology in to a continuous embodiment to produce CNT-g-CFs on the tow level without laborious pre-treatment of the fiber substrate. The morphology and mechanical properties of the continuous CVD synthesized CNT-g-CFs were characterized, as was the fiber-matrix interfacial shear strength in an epoxy matrix at the single fiber level. The results are compared, in detail, to literature data for

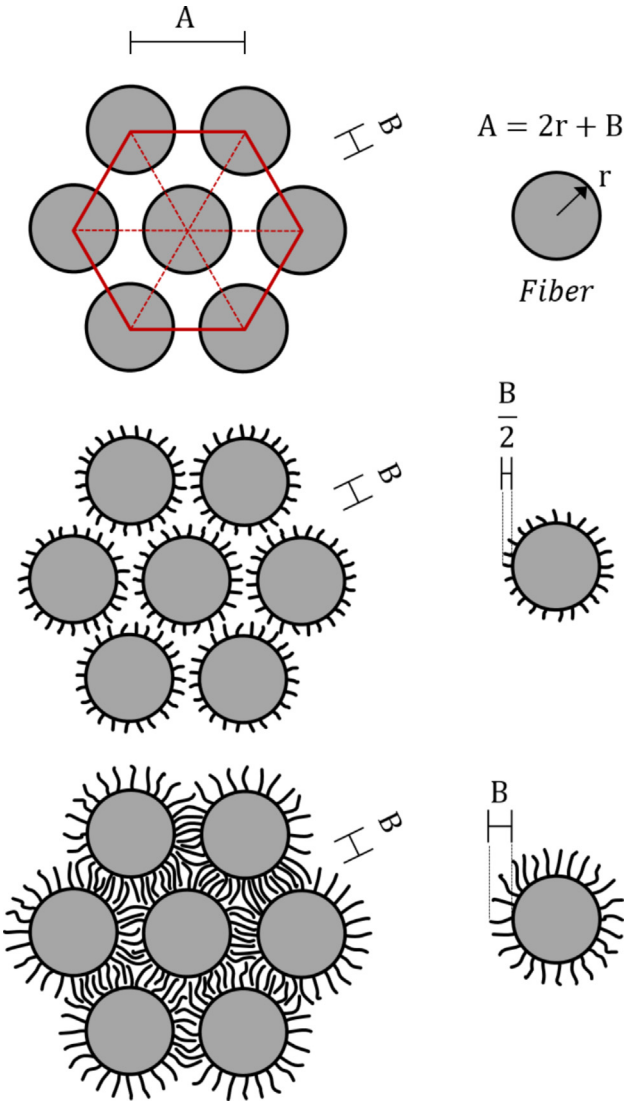

Fig. 1. Idealized hexagonal close packing in fiber reinforced composite for a fiber volume fraction 60%: (a) CFRC with fiber-fiber separation distance of B, (b) CNT-grafted-fibers with radial nanotubes from adjacent CNT-grafted-fibers, which just touch (nanotubes length = B/2), (c) CNT-grafted-fibers with nanotubes nesting between adjacent CNT-grafted-fibers (nanotube length ≥ B). (For interpretation of the references to colour in this figure legend, the reader is referred to the web version of this article.)

batch synthesized CNT-g-CFs.

2. Experimental

2.1. Materials

Commercially-available polyacrylonitrile (PAN)-based sized carbon fibers (AS4C-GP-12K-8, HS-CP-4000 grade) were supplied by Hexcel Composites (Duxford, GB) and used as a continuous tow containing 12,000 fibers. These carbon fibers were supplied with a 0.8–1.2 wt% sizing designed for an epoxy matrix,[†] and had a circular cross-section with a diameter of 6.9 μm.[‡] The analogous unsized polyacrylonitrile (PAN)-based carbon fiber (AS4-12K-7D, HS-CP-5000 grade) was also kindly provided by Hexcel Composites and had never been sized. This grade also consists of 12,000 fibers in a tow and had circular fiber cross-sections, but a diameter of 7.1 μm.[§] Iron(III) nitrate nonahydrate ($Fe(NO_3)_3{\cdot}9H_2O$, ≥98% ACS reagent, Sigma-Aldrich, GB), nickel(II) acetylacetonate (≥98%, VWR, GB) and ethanol (EtOH, > 99.7% BDH Prolabo, VWR, GB) were used to prepare the catalyst precursor. Nitrogen gas (99.998 vol% min), premixed hydrogen in nitrogen (N_2 97.6 vol% and H_2 2.4 vol%, C certificate (±) 5% level of analysis) and premixed acetylene in nitrogen (N_2 98.7 vol% with C_2H_2 1.3 vol%, C certificate (±) 5% level of analysis) were used for continuous CVD CNT synthesis. All gases were purchased from BOC Gases, GB. Graphite foil, approximate dimensions 100 mm × 180 mm × 0.2 mm was used as counter electrode (99.8%, C1179, Advent Research Materials Ltd, GB). Bisphenol-A (DGEBA) based liquid epoxy EP-828 from Netmro, US and Jeffamine T-403 (polyetheramine) curing agent from Huntsman, US were used as matrix for the pull-out test. A similar resin system was purchased from Polymer Gvulot Ltd., IL for the fragmentation test. Carbon fibers and all chemicals were used as-received.

2.2. Catalyst precursor deposition on carbon fibers

A 30 m long section of the sized carbon fiber 12 K tow was wrapped on a polytetrafluoroethylene frame and impregnated with catalyst precursor by submerging it for 2 min into a bi-catalyst precursor solution [48]. The sized carbon fiber was chosen as the substrate as it had been previously found to provide uniform CNT growth in the batch experiments [43]. The solution contained 2 wt% iron(III) nitrate nonahydrate and 2 wt% nickel(II) acetylacetonate in ethanol to obtain a molar ratio of Fe:Ni/1:1.6. The fibers were then dip washed in deionized water (18 MΩ cm at 25 °C) for 1 min and subsequently unwound on to a spool and dried in a fume hood at standard ambient atmospheric temperature and pressure.

2.3. Continuous synthesis of carbon nanotube-grafted-carbon fibers

Continuous CVD synthesis of CNT-g-CF was performed at 770 °C within a 2″ quartz tube enclosed in a hot-walled furnace. In an arrangement akin to the batch CNT-g-CF methodology previously reported [43], a potential difference can be applied to the carbon fiber substrate in a co-axial capacitor-like configuration. However, in the continuous embodiment, the electrical connection to the fiber tow was maintained by passing the fibers over a stainless-steel contact pin outside the furnace with the fibers passing through a tubular graphite foil counter electrode (earth), as shown in Fig. 2(a) and (b), which completed the capacitor-like circuit. When CNT-g-CF are synthesized with an applied potential difference, the voltages are presented in adjacent parentheses. An applied potential of 300 V was chosen for continuous CVD CNT-g-CF production, based on previous experience of batch production [43]. The catalyst precursor deposited carbon fiber tow was taken from ambient conditions, and pulled through the different CVD chambers within the reactor for continuous CNT synthesis growth. The collection of synthesized CNT-g-CF from the reactor was made in ambient conditions, using a motorized spool, which defines the linear uptake speed for the whole continuous line. The reactor was split into four gas exchange regions for heating, catalyst reduction, CNT synthesis and cooling. The tow passed through each region sequentially in an unhindered procession, at a constant speed of 1.2 m h^{-1}, Fig. 2(c). The dwell duration in each region was determined by the length of quartz tubes in each section. Inert gas sleeves were implemented to protect the fibers during heating and cooling stages in a nitrogen atmosphere (7500 sccm at 5 bar, both for 30 min). The catalyst precursor loaded onto the carbon fibers was reduced in hydrogen (premixed H_2 in N_2, 3400 sccm at 2 bar, for 10 min) to activate the catalyst for CNT growth in the central region (containing premixed C_2H_2 in N_2, 325 sccm at 2 bar, for

[†] Hexcel Composites. HexTow Carbon fiber. General Information. 2015:1–8.
[‡] Hexcel Composites. HexTow™ AS4C carbon fiber. Data Sheet. 2009:1–2.
[§] Hexcel Composites. HexTow™ AS4 carbon fiber. Data Sheet. 2009:1–2.

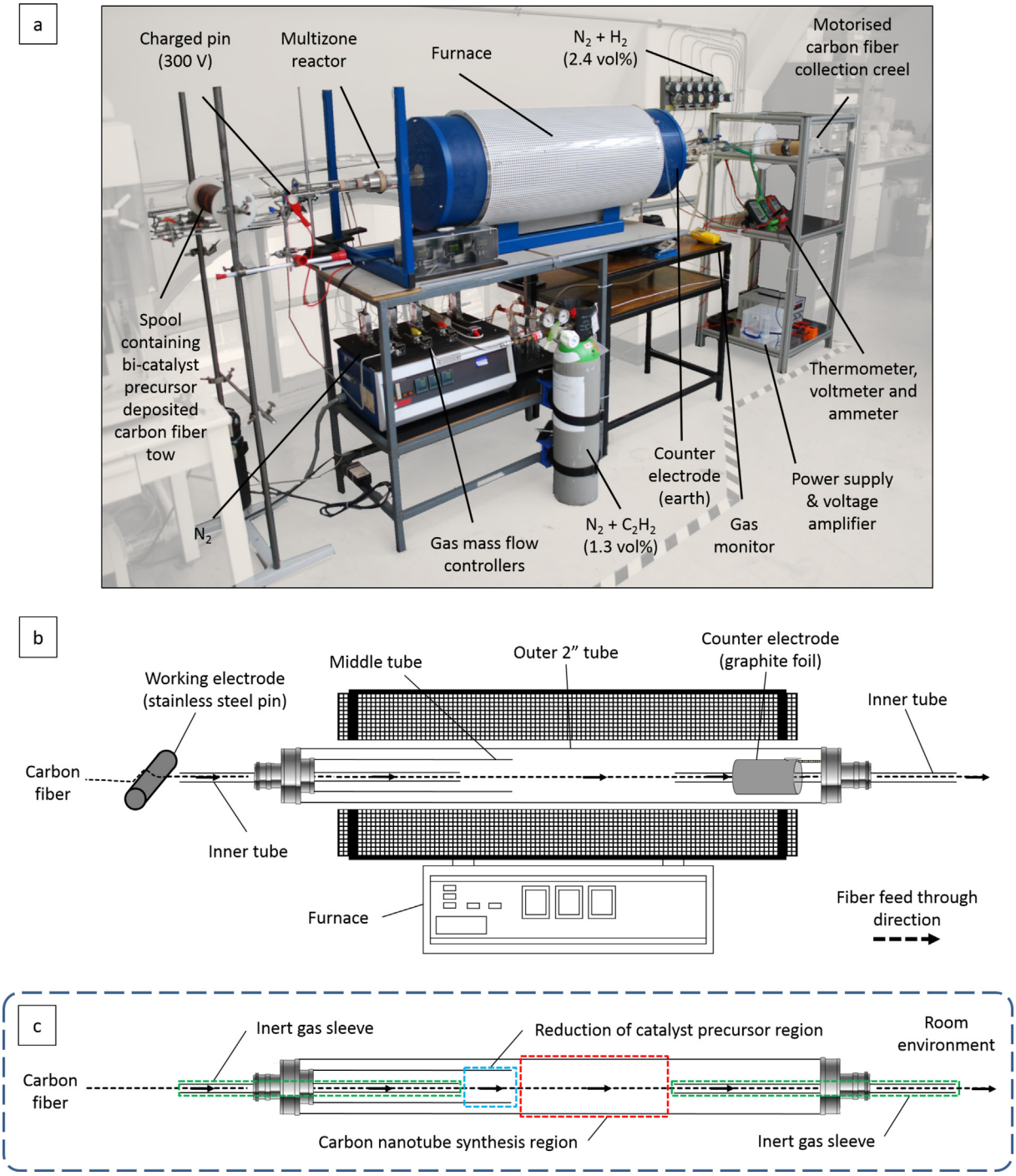

Fig. 2. Continuous CVD set-up for synthesis of CNT-g-CF (a) an overview photograph showing the fiber tow entry and exit from the reactor, (b) schematic of the electrical connections and concentric quartz tubes, which determine the reaction regions shown in (c). Not drawn to scale. (For interpretation of the references to colour in this figure legend, the reader is referred to the web version of this article.)

30 min). Further details of the CVD set-up, along with the determination of the volume percentages for flammable gases used and the circuit diagram, can be found in the SI S2, S3 and S4, respectively.

2.4. Characterization of the fiber morphology

As-received fibers, bi-catalyst precursor coated fibers, and CNT-g-CFs were assessed using a high-resolution field emission gun scanning electron microscope (SEM, Leo Gemini 1525 using SmartSEM software interface V05.05.03.00, Carl Zeiss NTS Ltd., GB) operated at 5 kV, and working distance ca. 10 mm. SEM specimens were prepared on Al stubs and adhered with silver DAG. SEM preparation products were sourced from Agar Scientific Ltd, GB. Fracture surfaces of single fiber composites were characterized by SEM using a SUPRA-55 VP (Carl Zeiss NTS Ltd., DE) or ULTRA-55 (Carl Zeiss NTS Ltd., DE). Micrographs were taken at an acceleration voltage of 3 kV or 5 kV and working distance between 4 mm and 5 mm. To prevent charging, the fractured single fiber composites were sputter coated (Edwards (US) S150) with a gold–palladium alloy prior to imaging. Grafted CNTs were imaged using transmission electron microscopy (TEM) using a JEOL-2010F electron microscope or a JEOL JEM-2100F. TEM images were collected using an acceleration voltage of 200 kV with specimens prepared in a

Table 1
Properties of carbon fibers and carbon nanotube-grafted-carbon fibers: diameter of the carbon fiber substrate d, CNT perpendicular thickness to fiber, CNT diameter d_{CNT}, specific fiber surface area A_{BET}, average intensity ratio I_G/I_D, and the temperature at which 99 wt% of original fiber mass and the temperature onset of combustion for the fiber. Values with ǂ, ◊, ¤ and ʒ refer to results obtained by SEM, TEM, Raman and TGA, respectively.

Carbon fibre samples	d ǂ [μm]	CNT perp. thickness to fiber◊ [nm]	d_{CNT} ◊ [nm]	A_{BET} [$m^2\ g^{-1}$]	Average I_G/I_D ¤	Temp. 99%ʒ [°C]	Temp. onsetʒ [°C]
As-received sized [43]	6.9 ± 0.2	N/A	N/A	0.28 ± 0.05	1.16 ± 0.02	529 ± 1	538 ± 1
As-received unsized	7.1 ± 0.2	N/A	N/A	0.34 ± 0.01	1.18 ± 0.04	567 ± 1	538 ± 1
Bi-catalyst precursor deposited [43]	6.9 ± 0.2	N/A	N/A	0.31 ± 0.05	1.09 ± 0.02	503 ± 1	469 ± 1
Cont. CNT-g-CF (0 V)	6.9 ± 0.2	N/A	N/A	0.26 ± 0.03	1.09 ± 0.02	534 ± 1	502 ± 1
Cont. CNT-g-CF (300 V)	7.0 ± 0.2	126 ± 69	9.1 ± 1.8	0.53 ± 0.05	1.06 ± 0.03	492 ± 1	501 ± 1

hinged TEM grid folded and secured using the provided latch (butterfly copper mesh, Agar Scientific Ltd., GB). Post-processing of micrographs to determine feature diameters was carried out using open-source Java software ImageJ (V. 1.45 s, U.S. National Institutes of Health, US) [49].

2.5. Characterization of the mechanical fiber properties

The mechanical properties of single fibers were measured using tensile tests and their matrix-fiber interfacial shear strength determined by single fiber fragmentation and single fiber pull-out tests in an epoxy matrix. Diameters of as-received, bi-catalyst precursor deposited, and as-synthesized CNT-g-CF were determined by SEM (Table 1).

2.5.1. Characterization of single fiber tensile properties

Single fiber tensile tests were carried out using a TST350 Tensile Stress Tester (Linksys32, V1.9.1, Linkam Scientific Instruments Ltd., UK) as described elsewhere [43,50], according to the British standard BS EN ISO 11566, 1996 [51] (Method B) in standard ambient atmospheric temperature and pressure using a 20 N load cell at crosshead speed of 15 μm s^{-1}. The device compliance (K) was determined to be 16.6 mm N^{-1}. Gauge-length dependent fiber strength fits are included in the results with the Weibull shape parameter determined from fiber strength populations using OriginPro (V8.6.0, Score method Blom, OriginLab Corp., USA, 2012) [52].

2.5.2. Characterization of model single fiber composites

Single fiber fragmentation/pull-out tests were conducted to determine the interfacial shear strength of carbon fibers/CNT-g-CFs in model epoxy composites. Composites were prepared with resin and curing agent mixed in stoichiometric proportions (1:0.42 w/w); the mixture was degassed in a vacuum oven at room temperature for 30 min; individual test preparation details are described below.

The fragmentation tests were performed using a computer-controlled Minimat tensile tester (Rheometric Scientific, Series 2000, 50 μm min^{-1} crosshead speed, 200 N load cell) mounted on a polarized optical microscope with video recording capabilities. A single carbon fiber was aligned along a dog-bone silicone mold, and kept taut by hanging a weight (approximately 0.6 g). The degassed epoxy was then cast into the mold and an additional degassing step was performed for 30 min. The composite was cured at 100 °C for 6 h. The resultant single fiber composite samples had a typical gauge cross-sectional dimension of ca. 1.45 mm × 1 mm and gauge length of ca. 12 mm. At least five specimens were tested for each configuration. Fiber break sites were observed *in-situ* under load (utilizing the birefringence effect) with the corresponding stress recorded at each instance. The average length of fiber fragments was determined to be the initial gauge length divided by the number of breaks counted plus one. Further increases of the applied stress cause the fiber to gradually break into shorter and shorter fragments. The fragment lengths progressively decreased, first linearly with the applied stress until a deviation from linearity occurred; further fragmentation followed until a saturation limit was reached, i.e. no further breaks occurred with increasing applied stress. Under low loads and those far below the saturation limit for fiber fragmentation, the probability of interaction between distant (on average) breaks along a fiber is low and the fragmentation test may be viewed as a "multiple tensile test" with independent samples, for which Weibull statistics apply. Assuming that the strength of a fiber obeys the Weibull weakest link model, the mean tensile strength σ_f of fibers of length L is described by:

$$\sigma_f(L) = \alpha L^{(-1/\beta)}\Gamma\left(1+\frac{1}{\beta}\right) = L^{(-1/\beta)}e^{\frac{intercept}{\beta}} \tag{1}$$

where α and β are the Weibull scale and shape parameters for strength, respectively, and Γ is the standard Gamma function. We may adopt Eq. (1) (in reverse form) to obtain the desired relationship between the average fragment length $\bar{l}$ and the average fiber stress $\bar{\sigma}_f$ described by:

$$\bar{l} = \alpha^{\beta}\bar{\sigma}_f^{-\beta}\left\{\Gamma\left(1+\frac{1}{\beta}\right)\right\}^{\beta} \tag{2}$$

The fiber stress $\bar{\sigma}_f$ is taken as $\bar{\sigma}_f = (E_f/E_m)\sigma_m$, where E_f and E_m are the fiber and matrix moduli, respectively, and σ_m is the measured stress (which can be determined from the force output) resulting from the applied strain. This assumption is valid as long as strain continuity at the fiber–matrix interface is maintained. The continuously monitored single fiber fragmentation approach yields two important results. First, away from the saturation limit, a plot of Eq. (2) in *ln–ln* form yields a straight line with slope equal to the Weibull shape parameter (β) of the embedded fiber. The Weibull scale parameter (α) of the fiber is readily obtained from the intercept of this line:

$$\beta[ln(\alpha) + ln\{\Gamma(1+\beta^{-1})\}] \tag{3}$$

Secondly, the interfacial shear strength can be calculated by adapting the classical Cottrell-Kelly-Tyson approach. As long as a fragment length remains greater than the critical length l_c, the fiber can break into smaller pieces, thus at saturation a range of fragment lengths exists, $0.5\ l_c < l_{sat} < l_c$, the average of which is $\bar{l}_{sat} = 0.75\ l_c$ (assuming the length distribution is Gaussian). From this saturation fragmentation length, assuming a constant interfacial shear stress, one can calculate the interfacial shear strength τ_i through the simple force balance:

$$\tau_i = \frac{d_f\bar{\sigma}_f(l_c)}{2l_c} \tag{4}$$

where d_f is the fiber diameter (measured for each sample from associated pull-out/embedded fiber after composite failure), and $\bar{\sigma}_f(l_c)$ is the ultimate strength of the fiber at the critical length, which can be calculated from Eq. (1) by using l_c instead of L.

For single fiber pull-out tests (detailed in SI S5) an in-house apparatus was used, following procedures previously reported [50,53,54]. The method involves embedding a single fiber using an in-house embedding device (detailed in SI S5), ca. 100 μm into a liquid epoxy resin filled aluminum screw followed by a cure cycle. A droplet of epoxy was placed into the screw and a clamped single fiber was maneuvered into the droplets' zenith. The fiber was then carefully submerged into the droplet, heated to 100 °C for 20 min using the integrated heater, then

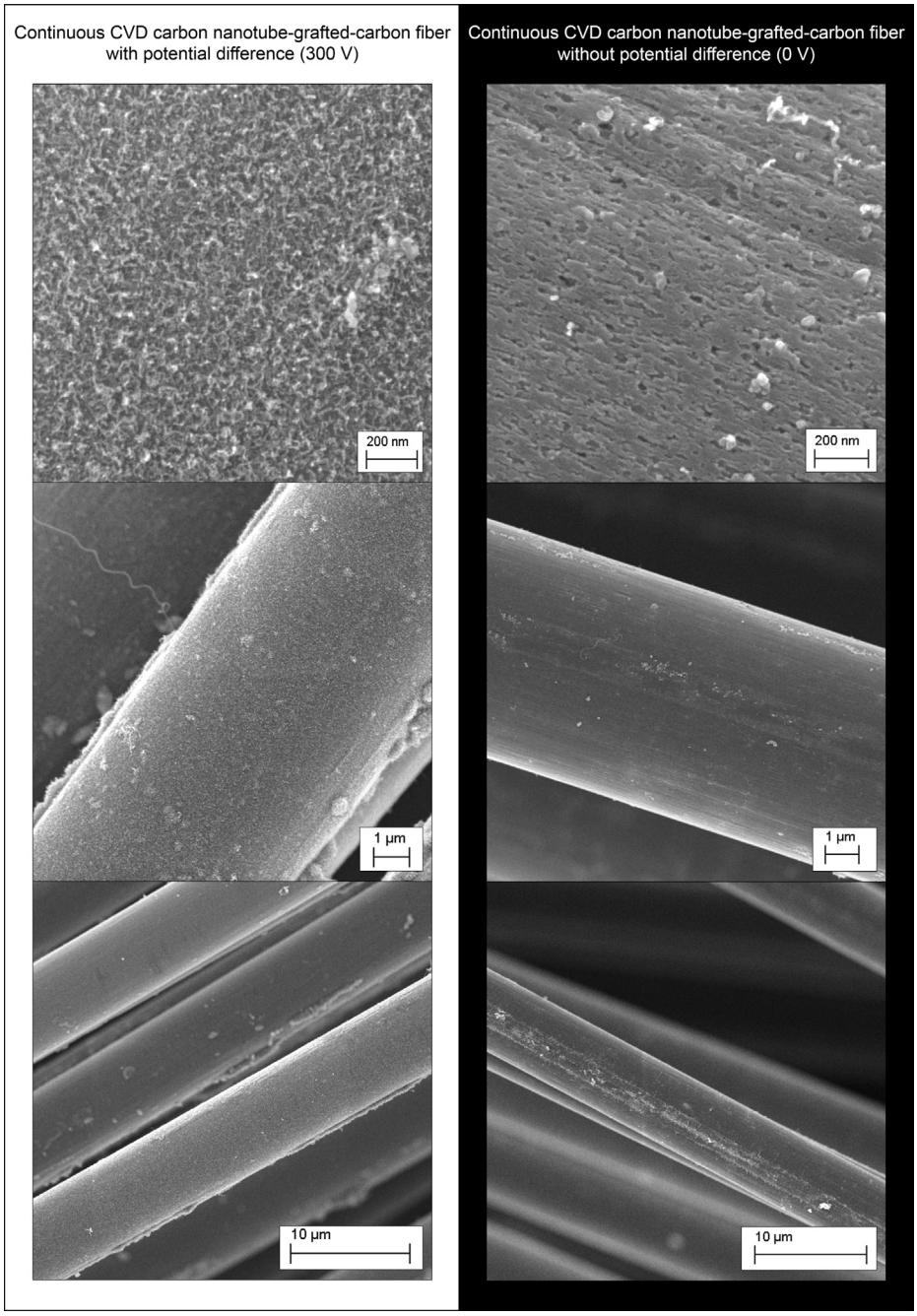

Fig. 3. SEM images of continuous CVD CNT produced with (300 V) and without (0 V) an applied potential difference, left and right, respectively. Additional CNT-grafted fibers, as-received sized fibers and unsized fibers and bi-catalyst precursor coated fibers micrographs can be found in SI S6.

removed and fully cured in an oven for 5 h 40 min. Then the sample is mounted onto a piezo-force sensor and the free end fixed to a piezo-translator. The pull-out test was performed on a stiff frame operated at cross-head speed of $0.2\,\mu m\,s^{-1}$ while the force-displacement was measured via computer interface, to accuracies of 0.1 mN and 1.8 nm, respectively. The apparent fiber pull-out interfacial shear strength τ_{app} was calculated from the peak pull-out force F_{max} and the embedded fiber area:

$$\tau_{app} = \frac{F_{max}}{\pi d_f l_e} \tag{5}$$

where d_f is the pulled-out fiber diameter (for each sample including any contribution from grafted CNTs) and l_e is the embedded fiber length. The free fiber length was approximately 100–150 µm, the embedded length and the fiber diameter were verified using optical and electron microscopy. The average pull-out interfacial shear strength was generated from at least 15 measurements for each specimen by a linear fit to the population of $F_{max} = f(A_e)$, i.e. the embedded fiber area.

2.6. Surface area characterization of fibers

The specific surface area of as-received fibers, bi-catalyst precursor coated fibers, and CNT-g-CFs was determined using the BET (Brunauer, Emmett and Teller) method following the ISO 9277 standard [55] using a Micromeritics TriStar Surface Area, Porosity Analyzer, and TriStar3000 V6.07 software (Micromeritics UK Ltd., UK) with oxygen-free nitrogen (99.998 vol%, BOC, UK). In order to achieve reliable results, the tests were conducted on samples which consisted of 12 K fiber

tows approximately 2 m long. The samples were degassed in nitrogen for at least 4 h at 80 °C before characterization.

2.7. Raman spectroscopic characterization of fibers

The evaluation of the graphitic structures through Raman analysis is non-destructive and commonly used to characterize the level of imperfections (disorder) in a sp^2 (graphene) framework via the intensity ratio of the G-mode (1582 cm^{-1}) to the D-mode (~1350 cm^{-1}) (I_G/I_D) [56]. Raman spectroscopy was performed on a LabRAM Infinity with 532 nm [2.33 eV] Nd-YAG green laser (LabSpec v4.18-06, Horiba Jobin Yvon Ltd., UK) in a backscattered geometry. Measured Raman spectra were processed with the background subtracted, then normalized to the G-mode and averaged using OriginPro (v8.6.0, OriginLab Corp., USA, 2012), with at least five independent locations sampled for each region.

2.8. Thermal gravimetric analysis of fibers

Thermal gravimetric analysis (TGA) was performed to determine whether the grafted CNTs or the CVD process affected the thermal stability of the carbon fibers. TGA was carried out on a Mettler Toledo TGA/DSC 1 with a GC200 flow controller, using STARe software v12.00C. The samples were heated under nitrogen from 30 °C to 100 °C at 35 °C min^{-1}, and then held isothermally at 100 °C for 30 min to dry, the gas was then changed to compressed air (60 sccm) and the temperature ramped to 850 °C at 10 °C min^{-1}.

3. Results and discussion

3.1. Microscopy and morphology

Whole tows of CNT-g-CF were successfully produced from pre-deposited catalyst precursor loaded carbon fiber, drawn through the continuous CVD system. Multiple, independent sections of CNT-g-CF tow were imaged by SEM (Fig. 3, additional micrographs in SI S6) for each sample (each region separated by a minimum of 0.4 m over a length of least 2 m,); quantitative analysis of the fiber diameters and average CNT length, with/without potential difference, are detailed in Table 1. Production of CNT-g-CF without an applied potential difference (0 V) resulted in irregular CNT-growth and pitting on the fiber surface (Fig. 3, right). CNT growth was significantly enhanced on carbon fibers when 300 V were applied (Fig. 3, left). The carbon fibers were covered with uniform CNTs (Fig. 3, left), which were relatively short ca. 125 nm and had diameters ca. 10 nm (TEM, Fig. 4). TEM images showed a range of structures grown at random orientations away from the carbon fiber surface, with a relatively disordered, multi-walled, internal structure ranging from tubular to hollow-core stacked nanocones, or partitioned stacked nanocones morphologies as defined

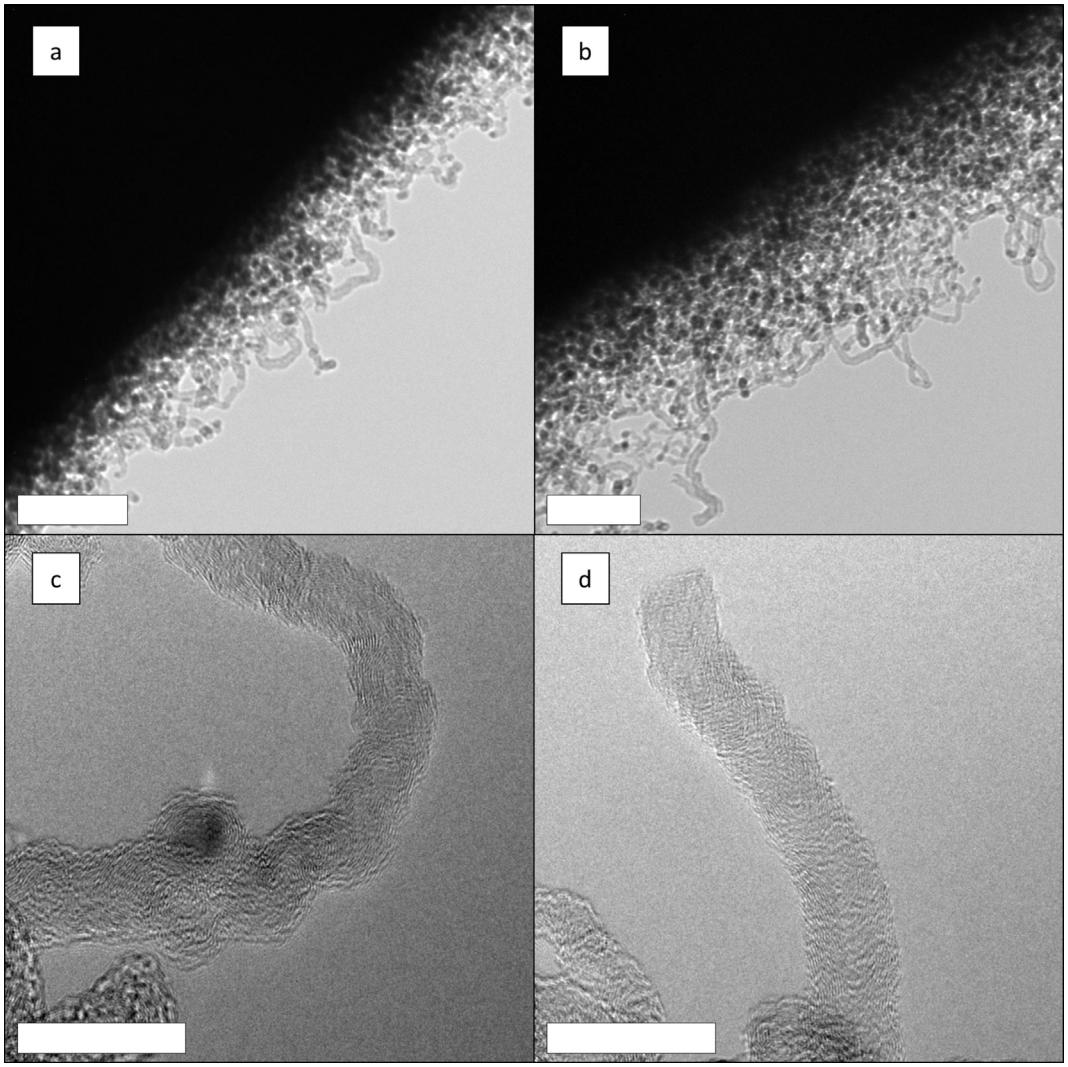

Fig. 4. TEM images of CNTs grafted to carbon fibers with an applied potential difference of 300 V (a) and (b) with 100 nm scale bar, and (c) and (d) with 20 nm scale bar.

by Suarez-Martinez *et al.* [57]. Electron micrographs of as-received sized/unsized and bi-catalyst precursor coated carbon fibers can be found in SI S6.

In the absence of acetylene (reductive conditions), the as-received sized carbon fibers appeared to be structurally unchanged after passing through the continuous CVD system (SEM, SI S7 and S8, with (300 V) and without (0 V) an applied potential difference, respectively). However, fiber damage and surface pitting were observed for bi-catalyst loaded fiber samples when no potential difference (0V) was applied under the same reductive conditions (SEM, SI S8, Fig. S.10(d)). Yet, when bi-catalyst loaded fibers were exposed to reductive conditions with a potential difference (300 V), there was less obvious fiber damage and minimal evidence of channeling [19,43] of catalyst particles into the carbon surface. Under these conditions, uniform catalyst particles (SEM, SI S7, Fig. S.9(d)) were formed with a similar diameter and distribution as the CNTs grown on the carbon fibers with an applied potential difference of 300 V.

In the batch operation mode of the CVD set-up [43], longer CNTs were grown than under continuous operation. In the continuous process, the effective gas flow rates were 84 sccm and 4.2 sccm for hydrogen and acetylene (at the same pressure, 2 bar, as the batch mode), respectively, which relates to a total reduction of the concentration of the reactive gases of 58% when compared to batch CVD CNT-synthesis conditions. This reduction in gas concentrations was necessary for safety reasons (SI S3). Moreover, the catalyst reduction time was kept constant at 10 min, but the effective CNT growth time was reduced by half to 30 min due to the length of the stable hot zone within the furnace (SI S2.6).

3.2. Tensile properties of (CNT-grafted-)fibers

In single fiber tensile tests, the tensile strength of the CNT-g-CF synthesized without an applied potential difference (0 V) was reduced (up to 20%) as compared to the as-received carbon fibers (Fig. 5, tabulated data SI S9). The loss in fiber tensile strength was attributed to the fiber surface damage caused by the catalyst pitting (Fig. 3). However, the tensile strength decreased to a lesser extent than for batch CVD [43], possibly due to the reduced residence time. The tensile strength of CNT-g-CF (300 V) was similar to that of as-received sized and bi-catalyst precursor coated control fibers, indicating that the application of a potential difference prevented damage during continuous CVD CNT growth. Unsized, as-received carbon fibers had a slightly higher strength, due to the inherent properties of the available grades. The tensile modulus of elasticity is a property associated with the fiber as a whole; when damage is sustained to the core of the fiber both the tensile strength and tensile modulus are reduced [30]. The tensile modulus was almost identical for all samples indicating that the fiber core remained unaffected by the CNT growth conditions. Fiber strength variability can be characterized using the Weibull shape parameter (Weibull modulus, β). All single fiber tensile specimens, with each sample set tested at three different gauge lengths, had similar Weibull distribution variance. The Weibull modulus for the majority of samples was in the range of 3.4 to 8.4, with the exception of CNT-g-CF (300 V), which had a higher Weibull modulus in the range of around 11, indicating a lower variance in strength between samples which is shown in the fit of the tensile data (Fig. 5(a)). A Weibull modulus of around 5 is common for carbon fibers [58], but the value can be as high as 14 for as-received carbon fibers, whilst Weibull moduli in the range of 5 to 7 have been reported for CNT-g-CF samples [59–61]. Single fiber fragmentation measurements identify high fiber strengths due to the short effective gauge. The ultimate fiber strengths at the critical length were similar for the as-received fibers, CNT-g-CF (300 V), and CNT-g-CF (0 V) samples (10.3 ± 0.3 GPa, 10.1 ± 0.4 GPa, and 10.6 ± 1.2 GPa, respectively). The inhomogeneous damage observed in the CNT-g-CF (0 V) case (Fig. 3, right), is not expected to affect the ultimate strength at the short effective gauge lengths.

3.3. Adhesion properties of (CNT-g-)carbon fibers to an epoxy matrix

Unsized, as-received, carbon fibers are often used as reinforcements for thermoplastic polymers. However, more commonly, carbon fibers are sized to protect fibers, coat surface flaws, improve ease of handling, and ease impregnation/wetting by thermosetting matrices. The interfacial shear strength of the fiber/epoxy matrix interface is often dramatically improved by a commercial sizing treatment when compared to the as-received unsized carbon fibers [62]. State-of-the-art, commercially sized fiber should therefore be used as bench-mark when measuring interfacial shear strength in epoxy matrices. The matrix choice is significant when considering interfacial properties, especially if there is poor compatibility between the reinforcing fibers and matrix. Substantial improvements are observed, for instance between thermoplastic matrices and carbon fibers, if the fiber surface is roughened/physically modified, with interfacial properties improving due to a mechanical interlocking mechanism [63], or through the redistribution of stresses at morphological features, such as CNT inclusions [10].

To determine if the CNTs grafted to carbon fibers could be effective for stress transfer in composites, fiber/matrix interfacial properties were characterized using single fiber fragmentation and single fiber pull-out tests. The matrix chosen for these studies was a common two-part bisphenol-A (DGEBA) based epoxy, which allows for comparison

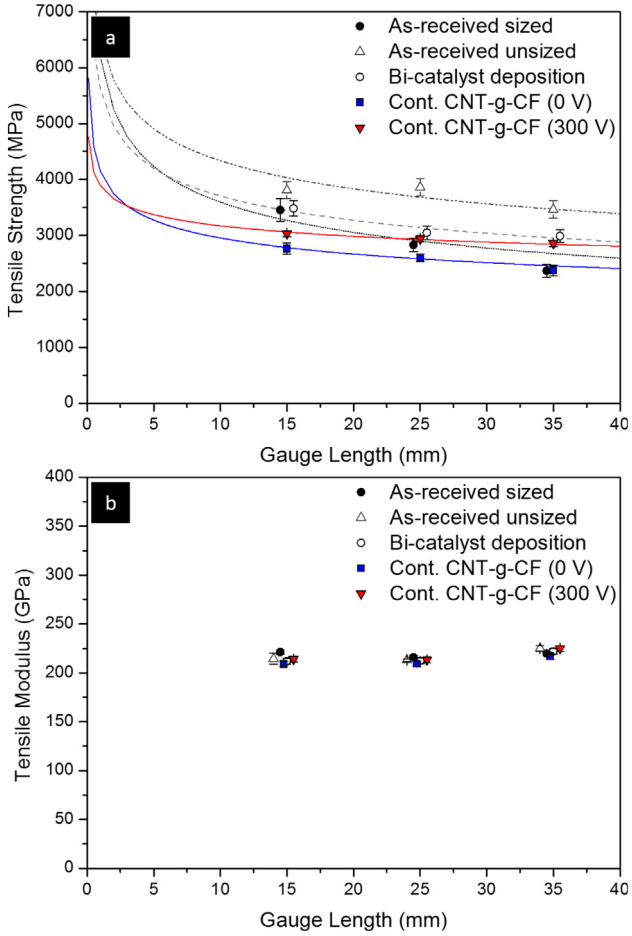

Fig. 5. Single carbon fiber tensile properties for as-received sized [43], as-received unsized, bi-catalyst precursor coated [43], and continuously CNT grafted carbon fibers with (300 V) and without (0 V) the application of a potential difference produced in the continuous set-up, (a) tensile strength (with gauge dependence fitted using the Weibull shape and scale parameters) and (b) tensile modulus. Data are slightly offset on the abscissa for clarity. (For interpretation of the references to colour in this figure legend, the reader is referred to the web version of this article.)

with current literature data.

Single fiber fragmentation: CNT-g-CFs synthesized with an applied potential difference (300 V) had a significantly improved interfacial shear strength in an epoxy matrix over as-received unsized and bi-catalyst precursor coated carbon fibers, by 71% and 117%, respectively, and a comparable interfacial shear strength to as-received sized carbon fibers (Fig. 6, tabulated data SI S10). CNT-grafted to carbon fibers in the absence of a potential difference (0 V) resulted only in a modest improvements of the interfacial shear strength over as-received unsized and bi-catalyst precursor coated carbon fibers, of 20% and 52%, respectively. Residues from catalyst precursor deposition for the bi-catalyst precursor coated fibers led to an overall reduction in interfacial shear strength by 21% when compared to unsized fibers, leading to premature debonding and pull-out of the fiber. The critical length of the different fibers at stress saturation reduced with increasing interfacial shear strength, as expected. Cross-sections of the single fiber model composites after the final rupture of the fragmentation test specimens are shown in Fig. 6(a)–(d), and in SI S10. The effect of sizing was

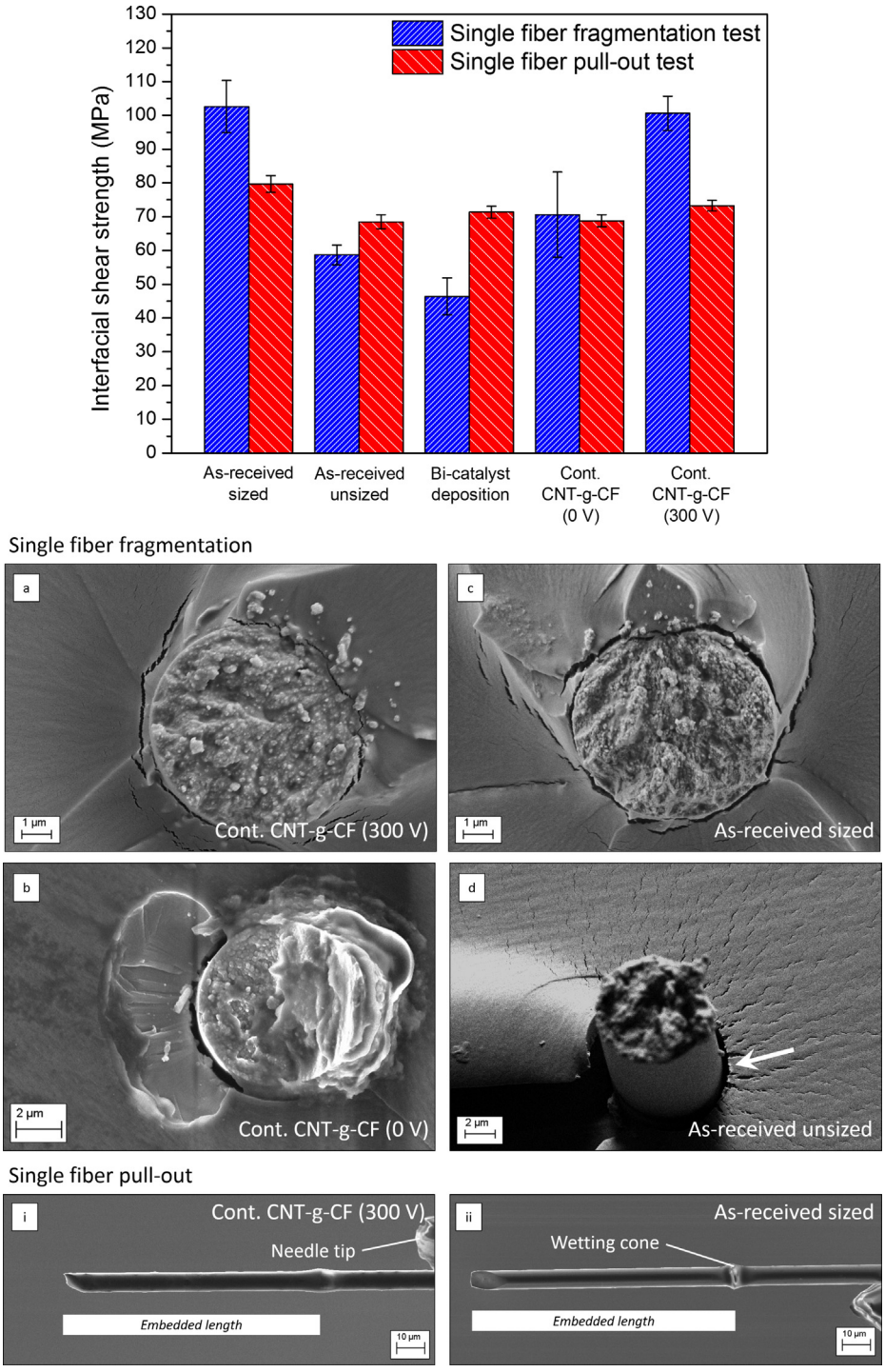

Fig. 6. (Top) Comparison of apparent interfacial shear strengths determined by single fiber fragmentation and single fiber pull-out tests. SEM images of cross-sections of fractured single fiber composites after fragmentation tests (a) CNT-g-CF (300 V), (b) CNT-g-CF (0 V), (c) as-received sized and (d) as-received unsized carbon fibers. SEM images of fiber surfaces pull-out from cured epoxy matrix droplets (i) CNT-g-CF (300 V), and (ii) as-received sized carbon fiber. (For interpretation of the references to colour in this figure legend, the reader is referred to the web version of this article.)

evident in the fracture cross-sections, with multiple textured microflow initiation sites and scarps extending into the matrix around the as-received sized fiber (Fig. 6(c)). The fracture plane of the matrix and the as-received sized fiber are coincident and consistent with a good interface between the two constituents, as confirmed by the high interfacial shear strength (102.6 ± 7.7 MPa). In contrast, as-received unsized fibers not only exhibited debonding (Fig. 6(d), indicated by a white arrow) but also fiber pull-out as a result of the poor compatibility between fiber and matrix, leading to a less effective stress transfer (58.7 ± 2.9 MPa). CNT-g-CF produced with an applied potential difference (300 V) exhibited a much better fiber/matrix adhesion; consequently, no debonding or pull-out were observed on fracture surfaces. Cracks in the matrix surrounding the CNT-g-CF (300 V) samples were observed (Fig. 6(a)) as a consequence of the stress transfer and the high interfacial shear strength (100.6 ± 5.1 MPa). Fracture surfaces for CNT-g-CF (0 V) (Fig. 6(b)) samples showed that partial debonding and fiber pull-out had occurred, which correlated with the lower interfacial shear strength (70.6 ± 12.6 MPa) when compared to CNT-g-CF (300 V).

Single fiber pull-out: The single fiber pull-out tests showed similar relative trends to the single fiber fragmentation tests (Fig. 6); however, the absolute values and relative spread are smaller. The interfacial shear strengths determined using single fiber fragmentation tests also relate to fiber strength, which can magnify variations; in contrast, only the interface, not the fiber, fails in a single fiber pull-out test. Tabulated results from the single fiber pull-out tests, additional micrographs, and the population linear fit for maximum force against embedded area are available in the SI S11. The interfacial shear strength between CNT-g-CF (300 V) and the epoxy matrix increased by 7% and 3% compared to as-received unsized and bi-catalyst precursor coated carbon fibers, respectively. The highest apparent interfacial shear strength was determined for the as-received sized sample, then CNT-g-CF (300 V) which was slightly lower, in this instance a decrease of 8%. The surface of the CNT-g-CF (300 V) pulled-out of was still coated by a thin layer of epoxy with CNTs visible below this layer (due to electron beam penetration into the surface) [64], suggesting that the interfacial failure occurred in the matrix region surrounding the CNT-grafted carbon fiber (Fig. 6(i), SI S11, Fig. S.13(a)), in agreement with fragmentation cross-sections (Fig. 6(a)). CNT-g-CF (0V) had one of the lowest interfacial shear strength in this series, resulting in generally clean failure surfaces of the single fiber model composites (SI S11, Fig. S.13(b)) but occasional small regions of CNTs were observed, attached to their surface (highlighted by an arrow). As the CNT-g-CFs (0 V) were passed through the furnace at high temperatures no sizing remained; moreover, the coverage of the fibers with CNTs was poor and, leading to a poor interaction with the epoxy matrix. Bi-catalyst precursor coated fibers showed a slight improvement over as-received unsized fibers, but lower than as-received sized fibers, suggesting that the catalyst precursor deposition did not remove the sizing completely (confirmed by TGA, Section 3.6).

Numerous papers have been published investigating the adhesion between CVD synthesized CNT-g-CF and polymer matrices (Tables 2 and 3). Although the definition of the fiber diameter is critical when determining the apparent interfacial shear strength of CNT-g-CF, the actual fiber diameter is often unclear or ill-defined in the literature. There are two approaches, using the overall CNT-g-CF diameter, which includes the cross-sectional area containing the CNTs [60] or only the diameter of the fiber substrate [18,59,65–68]. There are no specific standards for either single fiber fragmentation tests nor single fiber pull-out tests, yet there is a large body of literature for traditional fiber-matrix systems [69]. Relative differences between a baseline sample and modified samples are typically preferred rather than absolute values due to large testing variability. However, the choice of a suitable baseline sample is also problematic; whilst most researchers choose the as-received starting fiber, if this control is unsized or desized then the absolute values reported are only an improvement over the untreated/industrially treated carbon fiber surface [70], which potentially can have inherently poor fiber-matrix compatibility [71]. It may be more appropriate to include a sized fiber reference, depending on the system. The most prominent method to determine the fiber-matrix interfacial shear strength is the single fiber fragmentation test. In comparison with the literature (Fig. 7), the interfacial shear strength of CNT-g-CF (300 V) determined by single fiber fragmentation is amongst the highest values reported.

Generally, it can be seen from the literature that an increase in fiber/matrix interfacial shear strength is reported when CNT-grafted

Table 2
Reported apparent interfacial shear strength (IFSS), critical fiber length (l_c), fiber strength at critical length (σ_{lc}), fiber diameter (d), CNT-grafted-carbon fiber (CNT-g-CF), percentage difference of IFSS for baseline and CNT-grafted-CF (% dif.) determined from single fiber fragmentation tests for CNT-grafted-carbon fibers compared to controls.

			Carbon fiber (Baseline)				Carbon nanotube-grafted-carbon fiber				
Fiber substrate		Matrix	IFSS (MPa)	l_c (μm)	σ_{lc} (GPa)	d (μm)	IFSS (MPa)	l_c (μm)	σ_{lc} (GPa)	d_f (μm)	% dif.
Single fiber fragmentation test											
Amoco T300 [65]	Desized	P(VEAc)	2.90	2340 ± 40	–	4	13.78	2340 ± 40	–	–	375
Granoc YS-50-30S [72]	Desized	Epoxy	–	450 ± 80†	–	7†	–	–	–	–	15
Toray M40B [67]	Unsized	Epoxy	28.4	444	3.83	6.6	31.5	395	3.77	–	11
Hexcel IM7 [61]	Unsized	PMMA	12.5 ± 0.2	1750 ± 40	7.36	5.2	15.8 ± 0.4	1310 ± 40	7.07	5.2	26
Toray T300 [73]	Desized	Epoxy	17.4	760	3.53	7.5	47.8♣	320	4.07	7.5	175
Grafil 34-700 [74]	Unsized	Epoxy	–	600 ± 90†	–	7	–♣	–	–	–	–
Toray M40B [75]	Unsized	Epoxy	28.1 ± 5.5	448 ± 124	3.77 ± 0.06	6.6	32.0 ± 6.1	395 ± 115	3.83 ± 0.05	6.6†	14‡
TohoTenax HTR40 [23]	Unsized	Epoxy	35.4 ± 3.91	810 ± 100	8.21 ± 0.68	7†	37.4 ± 4.00♣	800 ± 130	8.48 ± 0.48	7†	6‡
Thornel T650 [66]	Sized	Epoxy	> 101.6	< 383	10.59	7.3	86.6♣	229	5.98	6.5	−15
Cytec T-300 [60]	Sized	Epoxy	36.9 ± 8.3	660 ± 120	6.8 ± 0.7	7 ± 0	70.0 ± 12.5	480 ± 80	3.3 ± 0.35	17.1 ± 0.4	90
UKN-M [68]	Sized†	Epoxy	28 ± 5	772 ± 45†	5.7 ± 1	7.5 ± 0.5	65 ± 9♣	262 ± 15†	4.6 ± 0.8	7.5†	132
Toray T700SC-50C [59]	Sized†	Epoxy	15.94 ± 2.01	980 ± 123	4.400	7	91.52 ± 10.89	305 ± 34	5.732	7	474
Cytec T-300 [18]	Sized	Epoxy	53.2 ± 6.0	440 ± 50	6.6 ± 0.2	7	65.7 ± 9.9	310 ± 40	5.7 ± 0.6	7	24
Toray T700S [76]	Sized	Epoxy	20.1 ± 1.06	826 ± 39.0	4.80 ± 0.03	7	66.0 ± 4.16	277 ± 14.3	5.22 ± 0.05	7†	228
Hexcel AS4C-GP-12K-8 (this work)	Sized	Epoxy	102.6 ± 7.7	345.6 ± 30.6	10.3 ± 0.3	7.0	100.6 ± 5.1	351.0 ± 19.7	10.1 ± 0.4	7.0	−2‡

Key: ‡ = mean values generated are within error, when error is presented. Unsized i.e. never sized as-received, Sized by manufacturer, Desized the as-received size is removed. P(VEAc) = polyvinylethylacetate, PMMA = poly(methyl methacrylate), † = details not readily available or specified in text and are taken from graphs using Graph Grabber (V1.5.5, Quintessa Ltd, UK), previous papers, or from a manufacturer data sheet. ♣ = additional coating on the carbon fiber $MgSO_4$, SiO_2, Al_xO_y or pyrolytic carbon, polymeric functional coating poly(styrene-alt-[dipotassium maleate]), for example. CNT-g-CF values detailed in each instance are highest reported with as-received sized base-lines sample presented where available, in preference over unsized/desized baselines.

Table 3
Reported apparent interfacial shear strength (IFSS), embedded fiber length (l_e), maximum force (F_{max}), fiber diameter (d_f), CNT-grafted-carbon fiber (CNT-g-CF), tow diameter (d_{tow}), percentage difference of IFSS for baseline and CNT-g-CF (% dif.) for CNT-grafted-carbon fibers compared to controls for microdroplet-debonding, single fiber pull-out, single fiber push out and fiber bundle pull-out test.

			Carbon fiber (Baseline)				Carbon nanotube-grafted-carbon fiber (CNT-g-CF)				
Fiber substrate		Matrix	IFSS (MPa)	l_e (μm)	F_{max} (mN)	d_f (μm)	IFSS (MPa)	l_e (μm)	F_{max} (mN)	d_f (μm)	% dif.
Microdroplet-debonding test ¥											
T300 [77]	Unsized	Epoxy	65 ± 3†	60–95†	85–135†	7.0 ± 0.1	135 ± 9†♣	58–85†	125–268†	7.0 ± 0.1	108
T300 [78]	Unsized	Epoxy	65 ± 3†	60–95†	85–135†	7.0 ± 0.1	126 ± 9†	58–85†	117–250†	7.0 ± 0.1	94
T-300 [79]	Sized	Epoxy	121	–	–	–	166	–	–	–	37
Tianniao HT CF [80]	Sized	Epoxy	43 ± 3†	–	–	7–10	55 ± 6†♣	–	–	–	28
Argon Ltd. UKN-M-12k-1 [81,82]	Sized	PUR	12.0 ± 0.9	–	146 ± 18	7	29.3 ± 1.1♣	–	320 ± 25	7.1–12†	144
Single fiber pull-out test											
Sigri C320.00A [50]	Unsized	Epoxy	75.2 ± 4.2	45–95†	62–162†	~7.5	118.3 ± 1.9	18–42†	43–119†	~7.5	57
Zoltek CF PET [83]	Desized	PET	–	1000	500	8–10	–	1000	1000	–	88
Inter-Turbine Advanced Logistics CF [84]	Sized†	Epoxy	27.4 ± 2†	–	28–51†	5–8	46.8 ± 1.1†	–	15–61†	–	71
Hexcel AS4C-GP-12 K-8 (this work)	Sized	Epoxy	79.7 ± 2.5	47.7–107.2	65–186	6.9	73.3 ± 1.6	30.8–88.8	47–165	7.0	−8
Single fiber push-out test											
Sigri C320.00A [50]	Unsized	Epoxy	49.5 ± 1.4	15–40	–	~7.5	50.6 ± 2.8	15–40	–	~7.5	2‡
T300 CF [85]	Sized	Δ	71 ± 16♣	250	475†	~7	> 116♣	250	> 640†	~10	63
T300 CF [40]	Sized	Δ	45 ± 17.3♣	270–300	235†	7.5	> 98♣	270–300	> 630†	25–30	118
Toray T700SC CF [86]	Sized	Epoxy	56.4 ± 5.3†	15–40	–	7	36.3 ± 8.3†	15–40	–	~8	−37.5
Fibre substrate		Matrix	IFSS (MPa)	l_e (mm)	F_{max} (N)	d_{tow} (mm)	IFSS (MPa)	l_e (mm)	F_{max} (N)	d_{tow} (mm)	% dif.
Fiber bundle pull-out test (3k tow)											
Grafil Pyrofil TR30S [37]	Sized	Epoxy	28.7 ± 2.87	200–2500†	6–139†	–	31.8 ± 5.01♣	400–3500†	5–69†	–	11‡

Key: ‡ = mean values generated are within error, when error is presented. Unsized i.e. never sized as-received, Sized by manufacturer, Desized the as-received size is removed. Carbon fiber (CF) used in-lieu when product details are omitted. PUR = polyurethane, PET = polyethylene terephthalate, Δ samples for single fiber push-out using T300 CF [40,85] are pyrolyzed after initial polymer infusion (phenolic resin, and polycarbosilane/xylene, respectively) then further densified with polycarbosilane. ¥ micro droplets of matrix on a fiber. † = details not readily available or specified in text and are taken from graphs using Graph Grabber (V1.5.5, Quintessa Ltd, UK), previous papers, or from a manufacturer data sheet. ♣ = additional coating on the carbon fiber $MgSO_4$, SiO_2, Al_xO_y or pyrolytic carbon, polymeric functional coating poly(styrene-alt-[dipotassium maleate]), for example. CNT-g-CF values detailed in each instance are highest reported with as-received sized baselines sample presented where available, in preference over unsized/desized baselines.

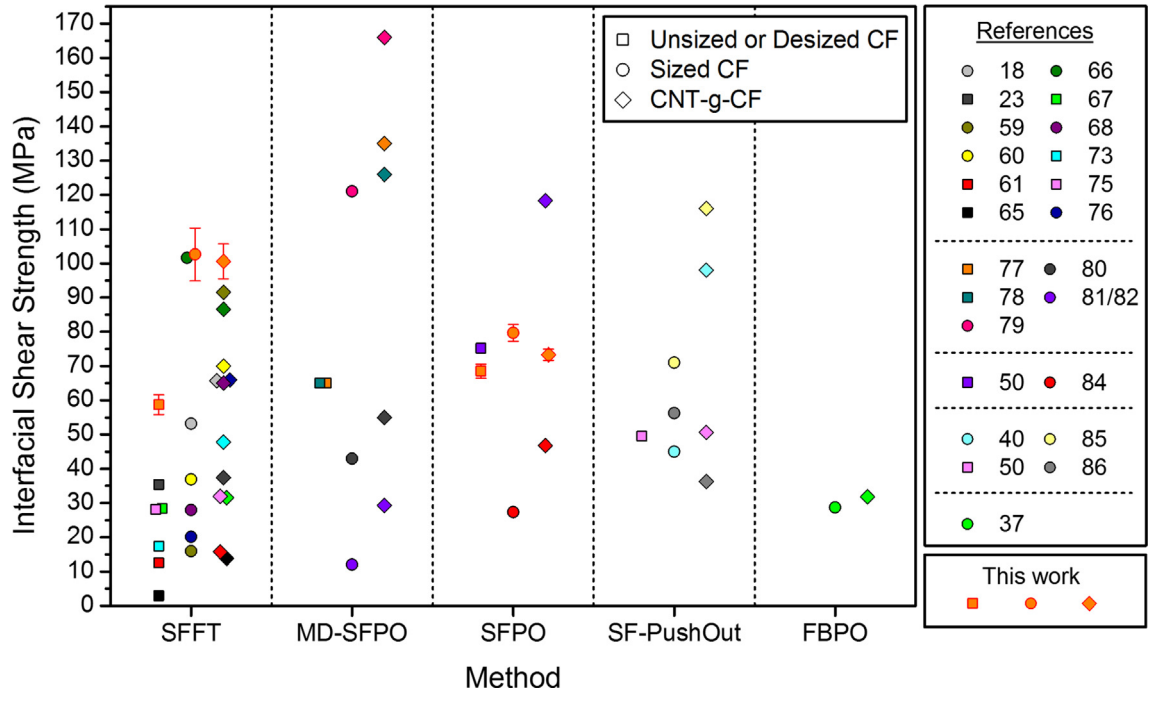

Fig. 7. Literature values of apparent interfacial shear strength determined from single fiber fragmentation tests (SFFT), microdroplet debond (MD-SFPO), single fiber pull-out (SFPO), single fiber push-out (SF-PushOut) and fiber bundle pull-out (FBPO) tests from Tables 2 and 3, including our values from this work (literature values have error bars omitted). (For interpretation of the references to colour in this figure legend, the reader is referred to the web version of this article.)

carbon fibers are used as reinforcement, when compared to control fibers, but the extent of the improvement varies dramatically, up to 474%, with an average of 84%. The most commonly studied matrices are epoxies, most likely due to ease of sample preparation, and practical relevance. When thermoplastic matrices are used, relative increases in interfacial shear strength between 26% and 375% have been reported, but the control fiber/matrix interfacial shear strengths are typically low ($< \sim 15$ MPa). The largest average improvements are observed by the single fiber fragmentation method, since the load is progressively transferred between the matrix and the fiber (up to fiber failure or local debonding); in other test methods, a single debonding event causes interfacial failure of the whole.

3.4. Surface area of (CNT-grafted-)carbon fibers

The specific surface areas for all samples were below 1 $m^2\ g^{-1}$ (Table 1), but these low values are expected for as-received and bi-catalyst precursor coated fibers. All samples showed a Type II adsorption isotherms (in SI S12) characteristic for a non-porous structure in accordance with the IUPAC classification [87]. The length of CNTs grown in the continuous CVD set-up were significantly shorter than those grafted onto carbon fibers in batch CVD reported in the literature [43], and yet still showed ~90% increased specific surface over the as-received sized fibers. By simple geometric arguments, assuming the CNTs to have a surface area of 260 $m^2\ g^{-1}$, the increase indicates that the CNT (300 V) loading is around 0.1 wt% relative to the carbon fiber. This value is consistent with the thin, porous layer of CNTs grafted to the fiber surface.

3.5. Raman spectroscopy analysis of (CNT-grafted-)carbon fibers

As-received sized/unsized and bi-catalyst precursor coated carbon fibers all had Raman spectra characteristic for PAN-based carbon fibers, exhibiting both D- and G-modes (I_G/I_D ratios tabulated in Table 1, combined and normalized spectra available in SI S13). For CNT-g-CF synthesized in the presence of an applied potential difference (300 V), the emergence of the 2D-mode (also known as G′ band) at ~2700 cm^{-1} in addition to a more prominent D- and G-mode sharpening [88] indicates that reasonably crystalline CNTs were grafted onto carbon fibers. There was a negligible difference in the Raman spectra for CNT-g-CF in the absence of an applied potential difference (0 V) over the as-received fibers, no mode sharpening was observed, indicating no significant CNT contribution.

3.6. Thermal stability of (CNT-grafted-)carbon fibers

TGA (data in SI S14) showed that the synthesized CNT-g-CFs (300 V) are stable through the range of temperatures used for composite manufacture. The weight loss at 400 °C for as-received sized and bi-catalyst precursor deposited carbon fiber samples was predominately due to the loss of sizing (applied by the manufacturer) and accounted for approximately 0.4 wt% for both fibers. The sizing remaining after deposition of the catalyst precursor explains the slight improvement in interfacial shear strength for bi-catalyst precursor coated over unsized as-received carbon fibers (Section 3.3). Whilst there was a small decrease in the onset degradation temperature (99 wt% of original mass in air, Table 1), ca. 490 °C, the CNT-g-CF (300 V) were stable well above the conditions required to process and cure typical epoxy matrices (typically 150–180 °C) and are even suitable for high temperature thermoplastics, such as polyetheretherketone (PEEK, 380–400 °C).[**]

[**] Victrex PLC. VICTREX® PEEK 450PF. Data sheet. 2014:1

3.7. Onset potential difference for enhanced carbon nanotube synthesis

Although the application of a potential difference of 300 V is sufficient to improve the synthesis of CNTs on carbon fibers, the continuous CVD set-up provides a convenient route to experimental investigation and optimization. As example, the minimum onset potential was established, by varying the applied voltage (0–200 V, in 50 V incremental steps) whilst using otherwise constant continuous CVD synthesis conditions for CNT-g-CF (Experimental Section 2), including catalyst precursor loaded substrate, gas flows, temperature, and dwell durations. A one-meter long section (of a continuous tow) was passed through the reactor for each set potential difference. SEM analysis (SI S15) showed that enhanced CNT growth was only observed at an applied potential difference exceeding 150 V, with increased CNT growth observed on further increasing the potential difference. The specific enhancement mechanism is unclear but is likely to include modifications of the catalyst mobility or changes to the catalyst (electro)wetting characteristics [89–91], Coulombic effects altering the catalytic activity/particle size and dissolution behavior, or a combination thereof. Further increases in the potential difference between electrodes are limited by the electrical breakdown threshold of nitrogen (arcing), which is also dependent on the specific electrode materials, geometries and displacement. These CNTs synthesis conditions are incompatible with generating or sustaining a plasma [43], the electrodes maintained a fixed potential difference, and no characteristic plasma glow was observed.

4. Conclusions

A continuous open–ended chemical vapor deposition (CVD) reactor has been developed for producing carbon nanotube–-grafted–carbon fiber (CNT-g-CF) in a spool to spool fashion. The application of a potential difference to the fibers *in-situ*, was critical to enable the growth of a homogenous, thin layer of nanotubes. This truly scalable manufacturing process, shown on the tow scale, crucially preserves the fiber mechanical, and fiber-matrix interfacial properties; both are critical factors for the successful use of CNT-g-CF for composite applications. The methodology could, in principle, be incorporated into traditional carbon fiber production. The carbon nanotubes grafted to carbon fibers had an average diameter ~10 nm and lengths ~125 nm, which are suitable for use in composites without reducing fiber volume fraction. The major benefit of the potential difference enhanced continuous CVD CNT–g-CF production is that it may be carried out without laborious pre–treatment(s) to the carbon fiber surface, an important step forward towards commercialization and improved properties. The potential benefits of such hierarchical reinforcement in composites are indicated by single fiber micromechanical tests; the fiber/matrix adhesion in epoxy was similar for CNT-g-CF synthesized with an applied potential difference (300 V) to those of commercially-sized carbon fibers, potentially approaching the shear strength of the matrix. The hierarchical reinforcements will be particularly relevant to systems where traditional modifications to fiber surfaces are underdeveloped, for instance in thermoplastic composite systems requiring high processing temperatures or high temperature use thermosets systems (polyimide, for example). They are also relevant to composites requiring enhanced electrical or thermal conductivity, for example for structural health monitoring, electromagnetic shielding, or improved fire performance.

Acknowledgements

The authors D.B.A., H.D.L., E.R.D., E.S.G., A.B., and M.S.P.S. would like to thank the UK Engineering and Physical Sciences Research Council (EPSRC) (EP/P502500/1), EPSRC Impact Acceleration: Pathways to Impact Award (EP/K503733/1) and Weizmann UK Programme Grant, The Weizmann Institute of Science, Hierarchical composites based on carbon nanotube fibres (2012-2015) for financial

support of this work. We thank Hexcel for supplying the AS4C and AS4 carbon fibers. Dr Jodie Melbourne and Dr Adam J. Clancy, NanoHAC Group, Imperial College London are acknowledged for their help with TEM and TGA, respectively. Keith Morley and LewVac LLP, GB and Mr Richard J. Wallington and Chemical Engineering Mechanical Workshop, Imperial College London are acknowledged for consultation and fabrication of the quartz metal fittings and assistance fabricating the line, respectively. H.D.W. and X.M.S. would like to acknowledge partial support from the G.M.J. Schmidt Minerva Centre of Supramolecular Architectures at the Weizmann Institute, and the China-Israel Science Foundations collaborative research grant. This research was also made possible in part by the generosity of the Harold Perlman family. H.D.W. is the recipient of the Livio Norzi Professorial Chair in Materials Science. All underlying data to support the conclusions are provided within the manuscript or supplementary information.

Declaration of interest

None.

Appendix A. Supplementary material

Supplementary data associated with this article can be found, in the online version, at https://doi.org/10.1016/j.compositesa.2018.05.027.

References

[1] P. Morgan, Carbon fibers and their composites. Cambridge solid state science series. Florida: Taylor & Francis; 2005. p. 1153. < https://doi.org/10.1201/9781420028744 > .
[2] Hull D, Clyne TW. An introduction to composite materials. 2nd ed. United Kingdom: Cambridge University Press; 1996.
[3] Qian H, Greenhalgh ES, Shaffer MSP, Bismarck A. Carbon nanotube-based hierarchical composites: A review. J Mater Chem 2010;20(23):4751–62. https://doi.org/10.1039/C000041H.
[4] Advani S, Shaffer MSP, Sandler J, Fan ZR, Liang Z, Wang B, et al. Processing and properties of nanocomposites. Singapore: World Scientific; 2007. p. 450. < https://doi.org/10.1142/9789812772473 > .
[5] Kulkarni M, Carnahan D, Kulkarni K, Qian D, Abot J. Elastic response of a carbon nanotube fiber reinforced polymeric composite: a numerical and experimental study. Compos B Eng 2010;41(5):414–21. https://doi.org/10.1016/j.compositesb.2009.09.003.
[6] Chatzigeorgiou G, Efendiev Y, Lagoudas D. Homogenization of aligned “Fuzzy Fiber” composites. Int J Solids Struct 2011;48(19):2668–80. https://doi.org/10.1016/j.ijsolstr.2011.05.011.
[7] Yang L, He X, Mei L, Tong L, Wang R, Li Y. Interfacial shear behavior of 3D composites reinforced with CNT-grafted carbon fibers. Compos A Appl Sci Manuf 2012;43(8):1410–8. https://doi.org/10.1016/j.compositesa.2011.11.012.
[8] Romanov VS, Lomov SV, Verpoest I, Gorbatikh L. Can carbon nanotubes grown on fibers fundamentally change stress distribution in a composite? Compos A Appl Sci Manuf 2014;63:32–4. https://doi.org/10.1016/j.compositesa.2014.03.021.
[9] Romanov V, Lomov SV, Verpoest I, Gorbatikh L. Inter-fiber stresses in composites with carbon nanotube grafted and coated fibers. Compos Sci Technol 2015;114:79–86. https://doi.org/10.1016/j.compscitech.2015.04.013.
[10] Romanov VS, Lomov SV, Verpoest I, Gorbatikh L. Modelling evidence of stress concentration mitigation at the micro-scale in polymer composites by the addition of carbon nanotubes. Carbon 2015;82:184–94. https://doi.org/10.1016/j.carbon.2014.10.061.
[11] Sebastian J, Schehl N, Bouchard M, Boehle M, Li L, Lagounov A, et al. Health monitoring of structural composites with embedded carbon nanotube coated glass fiber sensors. Carbon 2014;66:191–200. https://doi.org/10.1016/j.carbon.2013.08.058.
[12] Kim H. Enhanced crack detection sensitivity of carbon fiber composites by carbon nanotubes directly grown on carbon fibers. Compos B Eng 2014;60:284–91. https://doi.org/10.1016/j.compositesb.2013.12.063.
[13] Aravand MA, Shishkina O, Straumit I, Liotta AH, Wicks SS, Wardle BL, et al. Internal geometry of woven composite laminates with “fuzzy” carbon nanotube grafted fibers. Compos A Appl Sci Manuf 2016;88:295–304. https://doi.org/10.1016/j.compositesa.2016.06.010.
[14] Qian H, Kalinka G, Chan KLA, Kazarian SG, Greenhalgh ES, Bismarck A, et al. Mapping local microstructure and mechanical performance around carbon nanotube gafted silica fibres: methodologies for hierarchical composites. Nanoscale 2011;3(11):4759–67. https://doi.org/10.1039/c1nr10497g.
[15] Shui X, Frysz CA, Chung DDL. Electrochemical behavior of hairy carbons. Carbon 1997;35(10–11):1439–55. https://doi.org/10.1016/S0008-6223(97)00081-X.
[16] Kundalwal SI, Suresh Kumar R, Ray MC. Effective thermal conductivities of a novel fuzzy fiber-reinforced composite containing wavy carbon nanotubes. J Heat Transf 2014;137(1):012401. < https://doi.org/10.1115/1.4028762 > .
[17] Kepple K, Sanbornb GP, Lacassea PA, Gruenbergc KM, Readyd WJ. Improved fracture toughness of carbon fiber composite functionalized with multi walled carbon nanotubes. Carbon 2008;46(15):2026–33. https://doi.org/10.1016/j.carbon.2008.08.010.
[18] Lachman N, Qian H, Houllé M, Amadou J, Shaffer MP, Wagner HD. Fracture behavior of carbon nanotube/carbon microfiber hybrid polymer composites. J Mater Sci 2013;48(16):5590–5. https://doi.org/10.1007/s10853-013-7353-2.
[19] Baker RTK, Chludzinski Jr JJ, Sherwood RD. A comparison of the catalytic influence of nickel, iron and nickel-iron on the gasification of graphite in various gaseous environments. Carbon 1985;23(3):245–54. https://doi.org/10.1016/0008-6223(85)90109-5.
[20] Hata K, Futaba DN, Mizuno K, Namai T, Yumura M, Iijima S. Water-assisted highly efficient synthesis of impurity-free single-walled carbon nanotubes. Science 2004;306(5700):1362–4. https://doi.org/10.1126/science.1104962.
[21] Tomita A, Tamai Y. Hydrogenation of carbons catalyzed by transition metals. J Catal 1972;27(2):293–300. https://doi.org/10.1016/0021-9517(72)90271-0.
[22] De Greef N, Magrez A, Couteau E, Locquet J-P, Forró L, Seo JW. Growth of carbon nanotubes on carbon fibers without strength degradation. Phys Status Solidi (b) 2012;249(12):2420–3. https://doi.org/10.1002/pssb.201200148.
[23] Li R, Lachman N, Florin P, Wagner HD, Wardle BL. Hierarchical carbon nanotube carbon fiber unidirectional composites with preserved tensile and interfacial properties. Compos Sci Technol 2015;117:139–45. https://doi.org/10.1016/j.compscitech.2015.04.014.
[24] Naito K, Yang J-M, Xu Y, Kagawa Y. Enhancing the thermal conductivity of plyacrylonitrile- and pitch-based carbon fibers by grafting carbon nanotubes on them. Carbon 2010;48(6):1849–57. https://doi.org/10.1016/j.carbon.2010.01.031.
[25] Kim KJ, Yu W-R, Youk JH, Lee J. Degradation and healing mechanisms of carbon fibers during the catalytic growth of carbon nanotubes on their surfaces. ACS Appl Mater Interf 2012;4(4):2250–8. https://doi.org/10.1021/am3002499.
[26] Magrez A, Seo J, Kuznetsov V, Forro L. Evidence of an equimolar C_2H_2-CO_2 reaction in the synthesis of carbon nanotubes. Angew Chem Int Ed Engl 2007;46(3):441–4. https://doi.org/10.1002/anie.200603764.
[27] Steiner SA, Li R, Wardle BL. Circumventing the mechanochemical origins of strength loss in the synthesis of hierarchical carbon fibers. ACS Appl Mater Interf 2013;5(11):4892–903. https://doi.org/10.1021/am4006385.
[28] Kudo A, Steiner SA, Bayer BC, Kidambi PR, Hofmann S, Strano MS, et al. CVD growth of carbon nanostructures from zirconia: mechanisms and a method for enhancing yield. J Am Chem Soc 2014;136(51):17808–17. https://doi.org/10.1021/ja509872y.
[29] Tyagi PK, Janowska I, Cretu O, Pham-Huu C, Banhart F. Catalytic action of gold and copper crystals in the growth of carbon nanotubes. J Nanosci Nanotechnol 2011;11:3609–15. https://doi.org/10.1166/jnn.2011.3740.
[30] Boroujeni AY, Tehrani M, Nelson AJ, Al-Haik M. Hybrid carbon nanotube–carbon fiber composites with improved in-plane mechanical properties. Compos B Eng 2014;66:475–83. https://doi.org/10.1016/j.compositesb.2014.06.010.
[31] de Resende VG, Antunes EF, de Oliveira Lobo A, Oliveira DAL, Trava-Airoldi VJ, Corat EJ. Growth of carbon nanotube forests on carbon fibers with an amorphous silicon interface. Carbon 2010;48(12):3655–8. https://doi.org/10.1016/j.carbon.2010.06.006.
[32] Delmas M, Pinault M, Patel S, Porterat D, Reynaud C, Mayne-L'Hermite M. Growth of long and aligned multi-walled carbon nanotubes on carbon and metal substrates. Nanotechnology 2012;23(10):105604. https://doi.org/10.1088/0957-4484/23/10/105604.
[33] Moon C-W, Meng L-Y, Im S-S, Rhee K-Y, Park S-J. Improvement of the electrical conductivity of carbon fibers through the growth of carbon nanofibers. J Nanosci Nanotechnol 2011;11(7):6193–7. https://doi.org/10.1166/jnn.2011.4398.
[34] Patton ST, Zhang Q, Qu L, Dai L, Voevodin AA, Baur J. Electromechanical characterization of carbon nanotubes grown on carbon fiber. J Appl Phys 2009;106(10):104313–9. https://doi.org/10.1063/1.3253747.
[35] Storck S, Malecki H, Shah T, Zupan M. Improvements in interlaminar strength: a carbon nanotube approach. Compos B Eng 2011;42(6):1508–16. https://doi.org/10.1016/j.compositesb.2011.04.039.
[36] Tehrani M, Boroujeni AY, Luhrs C, Phillips J, Al-Haik MS. Hybrid composites based on carbon fiber/carbon nanofilament reinforcement. Materials 2014;7(6):4182–95. https://doi.org/10.3390/ma7064182.
[37] Pozegic TR, Jayawardena KDGI, Chen JS, Anguita JV, Ballocchi P, Stolojan V, et al. Development of sizing-free multi-functional carbon fibre nanocomposites. Compos A Appl Sci Manuf 2016;90:306–19. https://doi.org/10.1016/j.compositesa.2016.07.012.
[38] Vieira R, Pham-Huu C, Keller N, Ledoux MJ. New carbon nanofiber/graphite felt composite for use as a catalyst support for hydrazine catalytic decomposition. Chem Commun 2002;9:954–5. https://doi.org/10.1039/B202032G.
[39] Szmyt W, Vogel S, Diaz A, Holler M, Gobrecht J, Calame M, et al. Protective effect of ultrathin alumina film against diffusion of iron into carbon fiber during growth of carbon nanotubes for hierarchical composites investigated by ptychographic X-ray computed tomography. Carbon 2017;115:347–62. https://doi.org/10.1016/j.carbon.2016.12.085.
[40] Hu J, Dong S, Wu B, Zhang X, Zhou H, Wang Z, et al. Tailoring carbon fiber/carbon nanotubes interface to optimize mechanical properties of Cf-CNTs/SiC composites. Int J Appl Ceram Technol 2014;11(2):207–17. https://doi.org/10.1111/ijac.12100.
[41] Hu J, Dong S, Wu B, Zhang X, Wang Z, Zhou H, et al. Mechanical and thermal properties of Cf/SiC composites reinforced with carbon nanotube grown in situ. Ceram Int 2013;39(3):3387–91. https://doi.org/10.1016/j.ceramint.2012.08.072.
[42] Li K-Z, Song Q, Qiang Q, Ren C. Improving the oxidation resistance of carbon/

carbon composites at low temperature by controlling the grafting morphology of carbon nanotubes on carbon fibres. Corros Sci 2012;60:314–7. https://doi.org/10.1016/j.corsci.2012.03.031.
[43] Anthony DB, Qian H, Clancy AJ, Greenhalgh ES, Bismarck A, Shaffer MSP. Applying a potential difference to minimise damage to carbon fibres during carbon nanotube grafting by chemical vapour deposition. Nanotechnology 2017;28(30):305602. https://doi.org/10.1088/1361-6528/aa783f.
[44] de Villoria R, Hart AJ, Wardle B. Continuous high-yield production of vertically aligned carbon nanotubes on 2D and 3D substrates. ACS Nano 2011;5(6):4850–7. https://doi.org/10.1021/nn2008645.
[45] Malecki HC, Zupan M. Scalable continuous growth of carbon nanotubes on moving fiber substrates. Compos A Appl Sci Manuf 2012;43(11):1914–20. https://doi.org/10.1016/j.compositesa.2012.06.019.
[46] Craddock JD, Qian D, Lester C, Matthews J, Mansfield W, Patrick J, et al. Continuous processing of multi-walled carbon nanotube-studded carbon fiber tapes for enhanced through-thickness thermal diffusivity composites. J Nanosci Nanotechnol 2015;15(9):6852–5. < https://doi.org/10.1166/jnn.2015.11620 > .
[47] Wang Y, Raman Pillai SK, Che J, Chan-Park MB. High interlaminar shear strength enhancement of carbon fiber/epoxy composite through fiber- and matrix-anchored carbon nanotube networks. ACS Appl Mater Interf 2017;9(10):8960–6. https://doi.org/10.1021/acsami.6b13197.
[48] De Luca H, Anthony DB, Qian H, Greenhalgh ES, Bismarck A, Shaffer MSP. Non-damaging and scalable carbon nanotube synthesis on carbon fibres. 17th European conference on composite materials (ECCM17). Munich, Germany: Paper ID: PO-3-39; 2016. p. 6. ISBN: 978-3-00-053387-7.
[49] Schneider CA, Rasband WS, Eliceiri KW. NIH Image to ImageJ: 25 years of image analysis. Nat Meth 2012;9(7):671–5. https://doi.org/10.1038/nmeth.2089.
[50] Qian H, Bismarck A, Greenhalgh S, Kalinka G, Shaffer MSP. Hierarchical composites reinforced with carbon nanotube grafted fibers: the potential assessed at the single fiber level. Chem Mater 2008;20(5):1862–9. https://doi.org/10.1021/cm702782j.
[51] British Standards Institution. Carbon fibre – determination of the tensile properties of single-filament specimens. BS ISO 1996;11566:1–5.
[52] Stoner EG, Edie DD, Durham SD. An end-effect model for the single-filament tensile test. J Mater Sci 1994;29(24):6561–74. https://doi.org/10.1007/bf00354022.
[53] Hampe A, Kalinka G, Meretz S, Schulz E. An advanced equipment for single-fibre pull-out test designed to monitor the fracture process. Composites 1995;26(1):40–6. https://doi.org/10.1016/0010-4361(94)P3628-E.
[54] Meretz S, Auersch W, Marotzke C, Schulz E, Hampe A. Investigation of morphology-dependent fracture behaviour with the single-fibre pull-out test. Compos Sci Technol 1993;48(1):285–90. https://doi.org/10.1016/0266-3538(93)90145-7.
[55] British Standards Institution. Determination of the specific surface area of solids by gas adsorption – BET method. ISO 2010;9277:1–24.
[56] Dresselhaus MS, Dresselhaus G, Saito R, Jorio A. Raman spectroscopy of carbon nanotubes. Phys Rep 2005;409(2):47–99. https://doi.org/10.1016/j.physrep.2004.10.006.
[57] Suarez-Martinez I, Grobert N, Ewels CP. Nomenclature of sp^2 carbon nanoforms. Carbon 2012;50(3):741–7. https://doi.org/10.1016/j.carbon.2011.11.002.
[58] Bunsell AR, Renard J. Fundamentals of fibre reinforced composite materials. Bristol and Philadelphia: Institue of Physics Publishing Ltd; 2005. < https://doi.org/10.1201/9781420056969 > .
[59] Kim KJ, Kim J, Yu W-R, Youk JH, Lee J. Improved tensile strength of carbon fibers undergoing catalytic growth of carbon nanotubes on their surface. Carbon 2013;54:258–67. https://doi.org/10.1016/j.carbon.2012.11.037.
[60] Lachman N, Carey BJ, Hashim DP, Ajayan PM, Wagner HD. Application of continuously-monitored single fiber fragmentation tests to carbon nanotube/carbon microfiber hybrid composites. Compos Sci Technol 2012;72(14):1711–7. https://doi.org/10.1016/j.compscitech.2012.06.004.
[61] Qian H, Bismarck A, Greenhalgh ES, Shaffer MSP. Carbon nanotube grafted carbon fibres: a study of wetting and fibre fragmentation. Compos A Appl Sci Manuf 2010;41(9):1107–14. https://doi.org/10.1016/j.compositesa.2010.04.004.
[62] Paiva MC, Bernardo CA, Nardin M. Mechanical, surface and interfacial characterisation of pitch and PAN-based carbon fibres. Carbon 2000;38(9):1323–37. https://doi.org/10.1016/S0008-6223(99)00266-3.
[63] Zhang F-H, Wang R-G, He X-D, Wang C, Ren L-N. Interfacial shearing strength and reinforcing mechanisms of an epoxy composite reinforced using a carbon nanotube/carbon fiber hybrid. J Mater Sci 2009;44(13):3574–7. https://doi.org/10.1007/s10853-009-3484-x.
[64] Minhua Z, Bin M, Jae-Woo K, Luke JG, Xiaohong G, Tinh N, et al. New insights into subsurface imaging of carbon nanotubes in polymer composites via scanning electron microscopy. Nanotechnology 2015;26(8):085703. https://doi.org/10.1088/0957-4484/26/16/169601.
[65] Downs WB, Baker RTK. Modification of the surface properties of carbon fibers via the catalytic growth of carbon nanofibres. J Mater Res 1995;10(3):625–33. https://doi.org/10.1557/JMR.1995.0625.
[66] Sager RJ, Klein PJ, Lagoudas DC, Zhang Q, Liu J, Dai L, et al. Effect of carbon nanotubes on the interfacial shear strength of T650 carbon fiber in an epoxy matrix. Compos Sci Technol 2009;69(7–8):898–904. https://doi.org/10.1016/j.compscitech.2008.12.021.
[67] Boura O, Diamanti EK, Aggelis D, Barkoula N-M, Gournis D, Paipetis AS. Carbon nanotube growth on high modulus carbon fibers and interfacial charaterization. 14th European conference on composite materials. Budapest, Hungary: Paper ID: 749-ECCM14; 2010. p. 10.
[68] Tolbin AY, Nashchokin AV, Kepman AV, Malakho AP, Sorokina NE, Morozov VA, et al. Preparation of bicomponent fibers by surface modification with fibrous carbon nanostructure filler. Fibre Chem 2012;44(4):252–8. https://doi.org/10.1007/s10692-012-9441-5.
[69] Spragg C, Drazal L. Fiber, matrix, and interface properties. STP1290-EB ed. West Conshohocken, PA, USA: ASTM International; 1996. < https://doi.org/10.1520/stp1290-eb > .
[70] Chee Ho KK, Qian H, Bismarck A, Nicolais L. Carbon fiber: surface properties. Wiley Encyclopedia of Composites: John Wiley & Sons, Inc.; 2011. < https://doi.org/10.1002/9781118097298.weoc024 > .
[71] Armistead JP, Snow AW. Fiber/matrix interface studies using fragmentation test: ASTM international; 1996. < https://doi.org/10.1520/stp1290-eb > .
[72] Thostenson ET, Li WZ, Wang DZ, Ren ZF, Chou TW. Carbon nanotube/carbon fiber hybrid multiscale composites. J Appl Phys 2002;91(9):6034–7. https://doi.org/10.1063/1.1466880.
[73] Lv P, Feng Y-y, Zhang P, Chen H-m, Zhao N, Feng W. Increasing the interfacial strength in carbon fiber/epoxy composites by controlling the orientation and length of carbon nanotubes grown on the fibers. Carbon 2011;49(14):4665–73. < https://doi.org/10.1016/j.carbon.2011.06.064 > .
[74] Malecki H, Duffy M, Markkula S, Zupan M. Charaterization of hybrid carbon nanotube composite interfaces as a function of length scale. In: Minerals MaMS, editor. Materials fabrication, properties, charaterization, and modeling TMS 2011 140th annual meeting and exhibition: supplemental proceedings. Hoboken, N. J.: Wiley; 2011. p. 99–107. < https://doi.org/10.1002/9781118062142.ch12 > .
[75] Boura O, Diamanti EK, Grammatikos SA, Gournis D, Paipetis AS. Carbon nanotube growth on high modulus carbon fibres: morphological and interfacial characterization. Surf Interf Anal 2013;45(9):1372–81. https://doi.org/10.1002/sia.5292.
[76] Kim T, Kamey M, Natori J, Kawada H. Fabrication of CNTs grafted hierarchical multiscale composite and evaluation of its mechanical properties. ECCM16 – 16th European conference on composite materials. Seville, Spain: Paper ID: 0750; 2014. p. 8.
[77] An F, Lu C, Guo J, He S, Lu H, Yang Y. Preparation of vertically aligned carbon nanotube arrays grown onto carbon fiber fabric and evaluating its wettability on effect of composite. Appl Surf Sci 2011;258(3):1069–76. https://doi.org/10.1016/j.apsusc.2011.09.003.
[78] An F, Lu C, Li Y, Guo J, Lu X, Lu H, et al. Preparation and characterization of carbon nanotube-hybridized carbon fiber to reinforce epoxy composite. Mater Des 2012;33:197–202. https://doi.org/10.1016/j.matdes.2011.07.027.
[79] Chong R, Qianming G, Liqiu G, Xiaoming Z, Ji L. Analyses of reinforcing effects of in situ grown CNTs on carbon fibre fabric/epoxy composites at micro- and macroscale. Micro Nano Lett, IET 2012;7(3):240–3. https://doi.org/10.1049/mnl.2012.0065.
[80] Wang C, Li Y, Tong L, Song Q, Li K, Li J, et al. The role of grafting force and surface wettability in interfacial enhancement of carbon nanotube/carbon fiber hierarchical composites. Carbon 2014;69:239–46. https://doi.org/10.1016/j.carbon.2013.12.020.
[81] Алексеевич УС. МОДИФИЦИРОВАНИЕ УГЛЕРОДНОГО ВОЛОКНА УГЛЕРОДНЫМИ НАНОСТРУКТУРАМИ. Troitsk, Moscow, Russia: Technological Institute for Superhard and Novel Carbon Materials; 2016.
[82] Mordkovich VZ, Karaeva AR, Urvanov SA, Kazennov NV, Zhukova EA. Novel flexible composites reinforced with CNT-grafted carbon fibers. MRS Adv 2016;1(20):1453–8. https://doi.org/10.1557/adv.2016.192.
[83] Agnihotri P, Basu S, Kar KK. Effect of carbon nanotube length and density on the properties of carbon nanotube-coated carbon fiber/polyester composites. Carbon 2011;49(9):3098–106. https://doi.org/10.1016/j.carbon.2011.03.032.
[84] Du X, Xu F, Liu H-Y, Miao Y, Guo W-G, Mai Y-W. Improving the electrical conductivity and interface properties of carbon fiber/epoxy composites by low temperature flame growth of carbon nanotubes. RSC Adv 2016;6(54):48896–904. https://doi.org/10.1039/c6ra09839h.
[85] Hu J, Dong S, Zhang X, Zhou H, Wu B, Wang Z, et al. Process and mechanical properties of carbon/carbon–silicon carbide composite reinforced with carbon nanotubes grown in situ. Compos A Appl Sci Manuf 2013;48:73–81. https://doi.org/10.1016/j.compositesa.2013.01.014.
[86] Zhang L, De Greef N, Kalinka G, Van Bilzen B, Locquet J-P, Verpoest I, et al. Carbon nanotube-grafted carbon fiber polymer composites: damage characterization on the micro-scale. Compos B Eng 2017;126:202–10. https://doi.org/10.1016/j.compositesb.2017.06.004.
[87] Sing KSW, Everett DH, Haul RAW, Moscou L, Pierotti RA, Rouquerol J, et al. Reporting physisorption data for gas/solid systems with special reference to the determination of surface area and porosity. IUPAC 1985;57(4):603–19. https://doi.org/10.1351/pac198557040603.
[88] An F, Lu C, Guo J, Lu H. Preparation of CNT-hybridized carbon fiber by aerosol-assisted chemical vapor deposition. J Mater Sci 2012;47(7):3327–33. https://doi.org/10.1007/s10853-011-6172-6.
[89] Frieder M, Jean-Christophe B. Electrowetting: from basics to applications. J Phys: Condens Matter 2005;17(28):R705–74. https://doi.org/10.1088/0953-8984/17/28/R01.
[90] Quilliet C, Berge B. Electrowetting: a recent outbreak. Curr Opin Colloid Interf Sci 2001;6(1):34–9. https://doi.org/10.1016/S1359-0294(00)00085-6.
[91] Verheijen HJJ, Prins MWJ. Reversible electrowetting and trapping of charge: model and experiments. Langmuir 1999;15(20):6616–20. https://doi.org/10.1021/la990548n.